Valley incision by debris flows: Evidence of a topographic signature

J. Stock and W. E. Dietrich

Department of Earth and Planetary Science, University of California, Berkeley, California, USA

[1]   The sculpture of valleys by flowing water is widely recognized, and simplified models of incision by this process (e.g., the stream power law) are the basis for most recent landscape evolution models. Under steady state conditions a stream power law predicts that channel slope varies as an inverse power law of drainage area. Using both contour maps and laser altimetry, we find that this inverse power law rarely extends to slopes greater than ∼0.03 to 0.10, values below which debris flows rarely travel. Instead, with decreasing drainage area the rate of increase in slope declines, leading to a curved relationship on a log-log plot of slope against drainage area. Fieldwork in the western United States and Taiwan indicates that debris flow incision of bedrock valley floors tends to terminate upstream of where strath terraces begin and where area-slope data follow fluvial power laws. These observations lead us to propose that the steeper portions of unglaciated valley networks of landscapes steep enough to produce mass failures are predominately cut by debris flows, whose topographic signature is an area-slope plot that curves in log-log space. This matters greatly as valleys with curved area-slope plots are both extensive by length (>80% of large steepland basins) and comprise large fractions of main stem valley relief (25–100%). As a consequence, valleys carved by debris flows, not rivers, bound most hillslopes in unglaciated steeplands. Debris flow scour of these valleys appears to limit the height of some mountains to substantially lower elevations than river incision laws would predict, an effect absent in current landscape evolution models. We anticipate that an understanding of debris flow incision, for which we currently lack even an empirical expression, would substantially change model results and inferences drawn about linkages between landscape morphology and tectonics, climate, and geology.   *INDEX TERMS:* 1824 Hydrology: Geomorphology (1625); 1815 Hydrology: Erosion and sedimentation; 3250 Mathematical Geophysics: Fractals and multifractals; *KEYWORDS:* debris flows, erosion, incision, landscape evolution, stream power

1. Introduction

[2]   The sculpture of Earth's unglaciated valleys by water has long been explored to understand both the processes and rates that create and maintain valleys [e.g., *Playfair*, 1802; *Gilbert*, 1877; *Davis*, 1902; *Horton*, 1945]. These early workers recognized that strath terraces bordering rivers and the adjustment of tributaries to main stems are evidence that rivers incise valleys. These visible signs of lowering, and the fascination with river longitudinal profile shape led to early speculation by nineteenth century workers [e.g., *Gilbert*, 1877] that rivers cut through Earth's crust at rates determined by water discharge and channel slope (S) for a given substrate (K). The recognition that valley incision may transmit the effects of climate change and tectonism throughout the landscape has led to a renewed interest in the problem of bedrock river incision and its erosion laws. The first and simplest approach was to assume that fluvial processes cut most unglaciated valleys, and that lowering rate was either a function of boundary shear stress or stream power (ω). For instance, *Howard and Kerby* [1983] proposed that bedrock incision rate $\partial z/\partial t$ was a power function of shear stress applied to the bed by a moving fluid so that:

$$-\partial z/\partial t = K_1\tau^b = K_1(\rho_w gRS)^b \qquad (1)$$

where z is elevation (positive upward), K_1 is a measure of bed erodibility, τ is shear stress, b is unknown, ρ_w is fluid density, R is hydraulic radius and S is slope. In the spirit of *Bagnold* [1966], *Seidl and Dietrich* [1992] proposed that bedrock lowering rate was proportional to work/unit time done on the river bed (i.e., power) so that

$$-\partial z/\partial t = \omega^n = (\rho_w gQS)^n \qquad (2)$$

where n is an unknown exponent and Q is discharge. As reviewed by many others [e.g., *Sklar and Dietrich*, 1998; *Whipple and Tucker*, 1999], expressions (1) and (2) can be

parameterized in terms of drainage area and slope using hydraulic relations, so that they take the form

$$\partial z/\partial t = U - K\,A^m\,S^n \tag{3}$$

where U is rock uplift rate, S is slope, and m and n are exponents whose values are debated but may be calibrated by direct measurement of erosion rates [e.g., *Howard and Kerby*, 1983; *Seidl et al.*, 1994; *Whipple et al.*, 2000] or longitudinal profile fitting [e.g., *Seidl and Dietrich*, 1992; *Rosenbloom and Anderson*, 1994; *Stock and Montgomery*, 1999; *Snyder et al.*, 2000; *Kirby and Whipple*, 2001]. When rock uplift rate and lowering rate are balanced so that the valley long-profile is at steady state, the expression leads to the expectation that

$$S = [U/K]^{1/n}\,A^{-m/n} \tag{4a}$$

or

$$\log S = \log(U/K)^{1/n} - m/n \log A \tag{4b}$$

[3] Availability of topography as DEMs (digital elevation models) and the desire to invert landforms quantitatively for erosion rate invites much use of equation (3). The expression has been used to infer parameters in the stream power law from area-slope data (see above) and the response of river profiles to tectonism [*Snyder et al.*, 2000; *Lague et al.*, 2000; *Kirby and Whipple*, 2001] or climate change [*Tucker and Slingerland*, 1997; *Whipple et al.*, 1999]. Most recent landscape evolution models use some form of equation (3) to model valley incision, either by including the possibility of alluvial channels which require the calculation of the divergence of sediment transport [e.g., *Willgoose et al.*, 1991; *Howard*, 1994; *Tucker and Slingerland*, 1994; *Kooi and Beaumont*, 1996; *Howard*, 1997; *Tucker and Bras*, 1998; *van der Beek and Braun*, 1999] or by assuming that bedrock river incision is the dominant process shaping channel long-profiles [e.g., *Anderson*, 1994; *Whipple and Tucker*, 1999; *Whipple et al.*, 1999; *Davy and Crave*, 2000; *Willett et al.*, 2001]. This long (yet incomplete) reference list is a measure of the reliance placed upon area-slope formulations like equation (3) to answer questions of widespread interest, like the response of landforms to climate change or rock uplift.

[4] Yet, little attention is paid to the extent of the valley network in which the stream power law is valid. For instance, in the steeplands of the western United States we have not observed field evidence for long-term bedrock river incision (like a strath terrace) above valley slopes of 0.05–0.10, a region below which debris flows rarely travel, and where well-developed fluvial bed forms like step-pools occur [e.g., *Montgomery and Buffington*, 1997]. Nor is it obvious that the power law trend observed in area-slope plots of many rivers [e.g., *Flint*, 1974] can be projected upstream of the steepest reaches where strath terraces are commonly observed (e.g., Figure 1b). Upstream lies a steep valley network whose properties are largely unexplored, where other processes such as debris flows are capable of carving valleys (e.g., Figure 2). Here topography is convergent in planform, but valleys lack banks or other fluvial features that define channels (e.g., Figure 3). Hillslopes
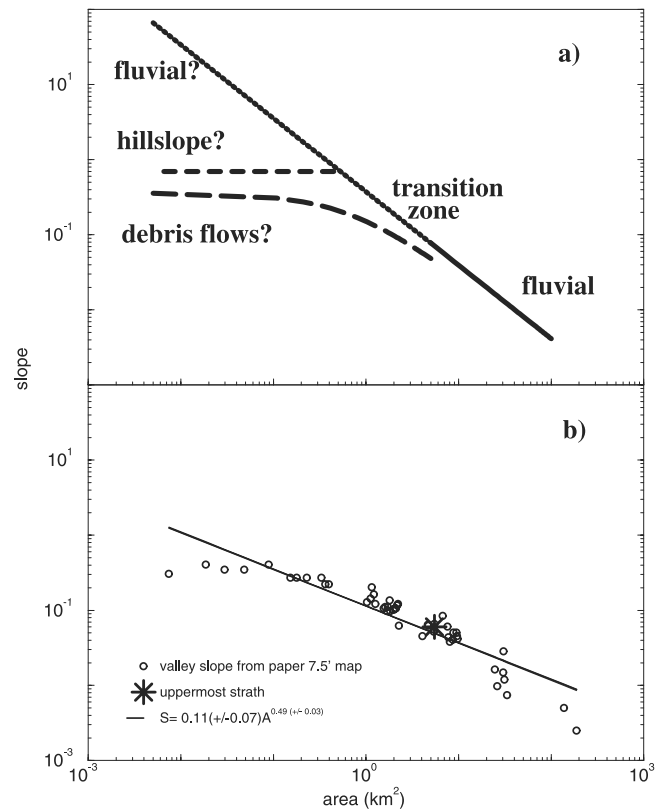
Figure 1. (a) Hypothetical topographic signatures for hillslope and valley processes. Area and slope are measured incrementally up valley main stem to the valley head. (b) Area-slope data from hand measurement of 1:24,000 topographic map and field observations of strath terraces, Deer Creek, Santa Cruz Mountains. Rightmost two data points are from 1:100,000 scale maps of San Lorenzo River. The data in Figure 1b appear to require more than one erosion law because a power law fit has nonrandom residuals.

deposit coarse, unsorted material in these valleys, leading some to call them colluvial valleys [*Montgomery and Buffington*, 1997]. The coarsest sediment size is often meters in dimension, many times the common water flow depth. In steeplands capable of generating landslides, the bulk of down valley sediment transport is by debris flows [e.g., *Dietrich and Dunne*, 1978; *Benda*, 1990]. Case studies in the Oregon Coast Range and other steeplands document that debris flows are rarely mobile below valley slopes of 0.02–0.05 (Table 1) although confinement, grain-size, fluid pressure, volume and junction angle also play a role [e.g., *Hungr et al.*, 1984; *Benda and Cundy*, 1990; *Iverson*, 1997]. The apparent lower limit of 0.02–0.05 in Table 1 corresponds to slopes reported for step-pool bed forms of *Montgomery and Buffington* [1997], while higher terminal slope values above 0.10 are typical of open slopes or fans in glaciated areas like British Columbia, Switzerland and Scandinavia. These observations lead to the expectation that valley network incision above slopes of 0.02–0.05 is influenced (at least in part) by debris flows.

[5] Perhaps because of the poor resolution of most DEMs, these valleys are often written about as if they were

Figure 2. Debris flow valley network in an Oregon Coast Range clear-cut. The combination of elevated water pressure during a 1996 storm and reduced root strength initiated landslides at valley heads that mobilized as debris flows, scouring sediment and Tyee sandstone (white areas) along the runout. Road at top right indicates scale.

part of hillslopes. For instance, some have found a change in power law slope (or a scaling break) in area-slope data from DEMs such that valley slope ceases to change below a certain drainage area. This has been inferred to represent a transition to hillslope processes (Figure 1a) [e.g., *Ijjasz-Vasquez and Bras*, 1995; *Moglen and Bras*, 1995; *Lague et al.*, 2000]. But this scaling break is inferred to occur at $0.1-1$ km^2, drainage areas at which valleys may occur. By contrast, others interpret the appearance of a scaling break as the topographic signature for debris flow valley incision [*Seidl and Dietrich*, 1992; *Montgomery and Foufoula-Geourgiu*, 1993; *Sklar and Dietrich*, 1998]. With the exception of *Howard* [1998], there are no proposals for a debris flow incision law or rule. When we started our investigations, little field evidence had been used to test either hypothesis. Examples of each are shown graphically in Figure 1a, from which two focused questions arise: what is the location of the scaling break (if any) and what is the form of the area-slope data above it? Since the form of area-slope data in steeplands could indicate a nonfluvial incision law, the location of the scaling break could define the extent of fluvial incision in steeplands. Given the widespread use of some form of stream power law, answers to these two questions have substantial implications for both landscape evolution models and geomorphic theory.

[6] In this paper we investigate the notion that debris flow valley incision in unglaciated steeplands has an area-slope

topographic signature distinct from that of bedrock river incision (Figure 1b). To do so, we avoid collection of data from hillslopes, and focus exclusively on valleys, which reflect concentrative erosional processes. We report results from visits to sites of recent debris flows where we observed evidence for bedrock lowering along their run out. Using both high- and low-resolution topography, we examine area-slope plots to see if they have a common form along the debris flow run out path. We also measure main stem area and slope for larger, unglaciated steepland valleys where the form of area-slope data follow fluvial power laws at large drainage areas, but may have a different form in the valley headwaters where we have mapped older debris flow deposits. We ask if the down valley disappearance of debris flow deposits and appearance of strath terraces (where present) has a consistent signature, such as a scaling break, that might separate fluvial from debris flow valley incision. Finally, we plot main stem valley slope and area from United States 1:24,000 and global 1:50,000 maps to investigate the generality of such signatures, and by inference the generality of debris flow valley incision in unglaciated mountain ranges.

2. Site Selection

[7] To investigate if debris flows imprint a topographic signature on valley longitudinal profiles, we visited sites of recent (<1 year-old) and historically recorded debris flows

Figure 3. View of bedrock valley bottom of Sullivan 1 (see Figure 5) in the Oregon Coast Range several months after scour by a debris flow. Note the surface parallel fractures in the Tyee Formation, some of which have been removed by the debris flow in the valley axis. In nearby untorrented valleys, unsorted hillslope deposits cover the bedrock.

in the western United States (Table 2). Although these sites were selected opportunistically, they span a wide range of climates and erosion rates from soil-mantled sandstone terrain lowering at 0.1 mm/yr (Oregon Coast Range), to semi-arid, bedrock-dominated gneissic terrain eroding at ∼1 mm/yr (San Bernardino Mountains). In these valleys (numbers 1–16 in Table 2) we measured area and slope from

laser altimetry (Sullivan, Scottsburg and Roseburg) or 1:24,000 USGS topography, and walked the run out of debris flows looking for evidence of bedrock erosion. In Table 2 we report deposition slopes measured in the field over the last 10 m of run out, or from high-resolution topography. These slopes tend to be higher than values from 1:24,000 maps for the same reach. Deposition slopes for

Table 1. Sampling of Slopes at Debris Flow Deposition

Slope	Confinement	Number of Flows	Data Source	Location	Reference
>0.02	valley/fan	summary	literature	global	*Costa* [1984]
0.02	fan	1	field or 1:24,000	San Gabriels, CA	*Sharpe and Nobles* [1953]
0.02–0.26	fan	14	survey over last 20 m	Japan (Yakedake)	*Suwa and Okuda* [1983]
0.03–0.05	valley/fan	1	1:24,000	Arizona	*Wohl and Pearthree* [1991]
0.03–0.11	valley	9	field survey	Oregon Coast Range	*Swanson and Lienkaemper* [1978]
0.03–0.14	valley	7	1:24,000	Oregon Coast Range	*Benda and Cundy* [1990]
>0.04	valley/fan	many	1:24,000	Appalachians, VA	*Morgan et al.* [1999]
0.04–0.27	valley/fan	26	1:10,000	Calabria, Italy	*Sorriso-Valvo et al.* [1998]
> 0.05	valley/fan	448	field survey	British Columbia	*Fannin and Rollerson* [1993]
0.05–0.20	fan	80	1:25,000	Switzerland, alpine	*Rickenmann and Zimmerman* [1993]
0.05–0.37	valley/fan	summary	literature?	Japan	*Ikeya* [1989]
0.05–0.55	valley	46	1:50,000	Oregon Cascades	this study, from P. Uncopher mapping
0.05–0.83	valley	many	1:24,000	Oregon Coast Range	this study, from Oregon Department of Forestry mapping
>0.07	valley	1?	1:24,000?	San Gabriels, CA	*Scott* [1971] as discussed by *Campbell* [1975]
0.07–0.09	fan	many	field or 1:24,000	San Gabriels, CA	*Morton and Campbell* [1974]
0.07–0.17	fan	many	field survey	New Zealand	*Pierson* [1980]
0.08–0.24	open slope/fan	9	field survey	Scandinavia	*Rapp and Nyberg* [1981]
0.09–0.16	valley	3	field or 1:24,000	West Virginia	*Cenderelli and Kite* [1998]
0.10	valley	1	field survey	Maui	this study
0.10	valley	1	1:24,000	Santa Monica, CA	*Campbell* [1975]
0.10–0.35	open slope/fan	9	field survey	Scandinavia	*Larsson* [1982]
0.11	valley	1	field survey	San Gabriels, CA	this study
0.12	fan	1	field or 1:20,000	Italy	*Berti et al.* [1999]
0.13–0.21	fan	>4?	field survey?	Colorado, alpine	*Curry* [1966]
0.14–0.31	valley/fan	7	1:25,000?	British Columbia, glacial	*VanDine* [1985]
0.16–0.20	valley/fan	4?	?	Swiss Alps	*Lewin and Warburton* [1994]
0.17–0.24	fan	5	field or 1:25,000	British Columbia, glacial	*Hungr et al.* [1984]
0.19–0.40	open slope/fan	9	survey?	French Alps	*Van Steijn et al.* [1988]

historic debris flows in the Wasatch Range are from fan slopes on 1:24,000 maps.

[8] With the goal of distinguishing river-cut valleys from those cut by debris flows, we selected river basins from steeplands with a range of rock uplift rate and climate including the San Gabriel Mountains, California Coast Range, King Range, Oregon Coast Range and Taiwan (valleys referred to in footnote d in Table 3). In these basins, we mapped the down-valley extent of existing debris flow deposits, and strath terraces to contrast fluvial with debris flow valley profiles. At all of the above sites, we compared the extent of the debris flows as judged from field mapping or historical accounts to area-slope plots of the same valley to look for a common topographic signature in the overlap. We also selected basins from unglaciated mountain ranges with reported debris flows in the United States, and from unglaciated steeplands around the world (Table 3). We constructed area-slope plots for these latter basins to explore the commonality of a potential topographic signature for debris flows.

[9] For sites of recent or historic debris flows, we measured area and slope from topographic maps along the run out path and mapped the spatial extent and style of bedrock erosion where present. We identified the downstream-most debris flow deposits along the valley main stem and compared area-slope data above and below this point to contrast the area-slope signature of debris flow basins with the proposed stream power law of fluvial basins. Although debris flows can stop on steeper slopes, we focused on the lowest gradients at which debris flows are commonly mobile because these reaches define the maximum potential influence of debris

flow incision by larger events. We defined the main stem as the valley with the larger drainage area at each tributary junction. We selected valleys of relatively uniform geology that contained both lower gradient rivers, and steeplands known to have debris flows. We chose main stem profiles without systematic changes in slope that might reflect deep-seated landsliding, faulting or lithologic changes. Exceptions are Marlow and Sullivan Creek, which have significant knickpoints on them that are not related to lithology. We included these basins because they have high-resolution DEMs and many recent debris flows in their catchments. The choice of main stem rather than tributary allows us to show the maximum possible extent of fluvial influence. We then mapped the extent of debris flow deposits and strath terraces onto 1:24,000 topography by walking the valley main stem. We used a conservative definition for debris flow deposits that required the following three observations: (1) matrix-support of large clasts in diamictons, (2) boulder berms, and (3) deposits located away from tributary junction fans. The intent was to avoid identifying coarse-grained fluvial deposits as debris flow deposits, and not to mistake small tributary fan deposits for along-valley debris flows. This means that we will underestimate long-term debris flow run-out because we do not include older, eroded debris flow deposits or matrix-poor debris flow deposits.

[10] To survey the commonality of a potential topographic signature for debris flows, we selected basins from around the world by (1) identifying a steepland region of relatively uniform valley density, (2) locating an area of uniform lithology within that region, and (3) selecting a basin within the region of uniform lithology with a concave

Table 2. Data for Valleys With Recent and Recorded Debris Flows, Located by USGS 1:24,000 Quadrangle Name

	Basin	Location	USGS 7.5' Quadrangle	Lithology	Average Rain, mm/yr	Erosion Rate, mm/yr	Approximate Date	Bedrock Scour Features	Deposition Slope	Debris Flow $a_0/(1 + a_1A^{a2})$	Erosion Rate[a]
1	Sul 1	Oregon Coast R.	Allegany	sandstone	1500–2500	0.07–0.1	1996/1997	abrasion, plucking	0.05	$1.03/(1 + 14.1A^{0.590})$	S,O: *Reneau and Dietrich* [1991], *Heimsath et al.* [2001]
1b	from 7.5' data									$1.05/(1 + 4.94A^{0.501})$	
2	Sul 2	Oregon Coast R.	Allegany	sandstone	1500–2500	0.07–0.1	1996/1997	abrasion, plucking	0.04	$0.725/(1 + 54.9A^{0.946})$	S,O: *Reneau and Dietrich* [1991], *Heimsath et al.* [2001]
3	Sul 3	Oregon Coast R.	Allegany	sandstone	1500–2500	0.07–0.1	1996/1997	abrasion, plucking	0.07	$0.773/(1 + 12.4A^{0.794})$	S,O: *Reneau and Dietrich* [1991], *Heimsath et al.* [2001]
4	Sul 4	Oregon Coast R.	Allegany	sandstone	1500–2500	0.07–0.1	1996/1997	abrasion, plucking	0.09	$0.712/(1 + 24.5A^{1.18})$	S,O: *Reneau and Dietrich* [1991], *Heimsath et al.* [2001]
5	Scott 1	Oregon Coast R.	Scottsburg	sandstone	1500–2500	0.2–0.3	1996/1997	abrasion, plucking	0.11	$0.797/(1 + 8.80A^{0.787})$	O: *Personious* [1995]
5b	from 7.5' data									$1.04/(1 + 9.74A^{0.779})$	
6	Scott 2	Oregon Coast R.	Scottsburg	sandstone	1500–2500	0.2–0.3	prehistoric	–	–	$0.830/(1 + 8.00A^{0.766})$	O: *Personious* [1995]
7	Scott 3	Oregon Coast R.	Scottsburg	sandstone	1500–2500	0.2–0.3	prehistoric	–	–	$0.859/(1 + 4.41A^{0.570})$	O: *Personious* [1995]
8	Silver Creek	Oregon Coast R.	Elk Peak	sandstone	1500–2500	0.07–0.1	1996/1997	abrasion, plucking	0.05	$0.468/(1 + 7.32A^{1.13})$	S,O: *Reneau and Dietrich* [1991], *Heimsath et al.* [2001]
9	Rose 1	Oregon Coast R.	Callahan	sandstone	1000–1500	~0.2	1996/1997	abrasion, plucking	0.10	$0.949/(1 + 8.25A^{0.868})$	O: *Personious* [1995]
10	Rose 2	Oregon Coast R.	Callahan	sandstone	1000–1500	~0.2	1996/1997	abrasion, plucking	0.10	$0.831/(1 + 69.7A^{1.97})$	O: *Personious* [1995]
11	Rose 3b	Oregon Coast R.	Callahan	sandstone	1000–1500	~0.2	1996/1997	abrasion, plucking	0.10	–	O: *Personious* [1995]
12	Yucaipa	San Bernardinos	Forest Falls	mica schist	610–1020	~1	1999	abrasion, plucking, chips	0.11	$0.707/(1 + 7.77A^{2.24})$	E: *Spotila et al.* [1999]
13	Joe's Canyon	Wasatch (Utah)	Spanish Fork Pk.	quartzite	510–1020	?	1998	abrasion, plucking, chips	0.05	$0.817/(1 + 2.97A^{0.468})$	Unknown
14	Steed	Wasatch (Utah)	Bountiful Peak	gneiss	640–1270	~1–2	1923, 1930	covered	0.05–0.11	$0.716/(1 + 1.27A^{0.532})$	E: *Armstrong et al.* [1999]
15	Rick's Ford	Wasatch (Utah)	Bountiful Peak	gneiss	640–1270	~1–2	1901?	covered	0.04–0.10	$0.740/(1 + 22.6A^{0.178})$	E: *Armstrong et al.* [1999]
16	Aa	Maui	Wailuku	basalt	3810–7620	?	historic?	covered	0.10	$1.06/(1 + 16.3A^{1.20})$	Unknown

[a]From S, suspended load; R, reservoir; E, fission track/cooling; U, marine terrace; and/or O, other.
[b]Values for equation (5) did not converge.

Table 3. Data for Valleys Used in Area-Slope Analysis From Contour Maps[a]

River	Location	Quadrangle	Lithology[b]	Average Rain, mm/yr	Erosion Rate, mm/yr	m/n	$[(-dz/dt)/K]^{1/n}$	Debris Flow $a_0/(1 + a_1A^{a2})$	Scaling Transitions Area, km²	Slope	Valley Head, m	River Head, m	Debris Flow Fraction	Erosion Rate Reference[c]
								1:24,000 Scale Maps						
Bear[d]	San Gabriels	Crystal Lake	granitic	1300–2000	0.7–1	0.57	0.431	$1.11/(1 + 2.59A^{0.637})$	7–10	.09–.15	2353	1365	0.42	E: Blythe et al. [2000]; O: Stock et al. (unpublished manuscript)
Alder	San Gabriels	Pacifico Mntn.	granitic	1300–2000	0.3–0.4	0.34	0.35	$0.617/(1 + 1.86A^{0.820})$	6–10	.05–.06	1890	1561	0.17	E: Blythe et al. [2000]
Sandymush	North Carolina	Sandymush	biotitic granitic gneiss	1200–1800	0.05–0.08	1.01	0.455	$0.919/(1 + 4.44A^{0.470})$	4–7	.08–.09	1500	817	0.46	R: Dendy and Champion [1978]
Cane	North Carolina	Montreat	metagreywacke	1200–1800	0.05–0.08	1.20	1.42	$0.333/(1 +.271A^{1.230})$	7–15	.06–.08	1756	1122	0.36	R: Dendy and Champion [1978]
Cook	Oregon Coast	Rogers Peak	basalt flows	2000–2500	0.4–0.8	0.42	0.085	$1.21/(1 + 12.1A^{0.723})$	5–6	.02–.04	707	280	0.60	O: Personious [1995]
Cummins	Oregon Coast	Yachats	basalt	1500–2000	0.2	0.71	0.12	$3.23/(1 + 24.2A^{0.467})$	4–5	.03–.04	610	146	0.76	S: Reneau and Dietrich [1991]; O: Personious [1995]
Marlow[d]	Oregon Coast	Golden Falls	micac. ss (Tyee)	1500–2500	0.07–0.1	–	–		–	–	–	–	–	S,O: Reneau and Dietrich [1991], Heimsath et al. [2001]
Sullivan[d]	Oregon Coast	Allegany	micac. ss (Tyee)	1500–2500	0.07–0.1	–	–		–	–	–	–	–	S,O: Reneau and Dietrich [1991]; Heimsath et al. [2001]
Indian	Oregon Coast	Cummins Peak	micac. ss (Tyee)	1500–2500	0.2	0.95	0.077	$0.571/(1 + 9.58A^{0.869})$	2–4	.02–.05	463	207	0.55	S: Reneau and Dietrich [1991]; O: Personious [1995]
Franklin	Oregon Coast	Scottsburg	micac. ss (Tyee)	1500–2000	0.2–0.3	0.73	0.132	$1.18/(1 + 11.9A^{0.543})$	4–6	.04–.07	2414	122	0.95	O: Personious [1995]
Deer[d]	Santa Cruz Mts.	Castle Rock Ridge	arkose, siltstone	1000–1500	0.15–0.3	0.90	0.31	$0.367/(1 + 1.37A^{0.942})$	5–6	.05–.09	866	463	0.46	R: Brown [1973]; S: Coats et al. [1982]; O: Perg et al. [2000]
Honeydew[d]	CA Coast	Shubrick Peak	greywacke	1300–3000	4	1.21	0.824	$0.429/(1 +443A^{1.650})$	4–10	.05–.06	1109	219	0.80	U: Merritts and Vincent [1989]
Elder[d]	CA Coast	Cahto Peak	greywacke	1800–2300	0.7	1.19	0.725	$0.516/(1 + 2.52A^{0.262})$	5–9	.06–.10	1244	457	0.63	U: Merritts and Vincent [1989]
Noyo[d]	CA Coast	Burbeck	greywacke	1000–1800	0.4	0.82	0.17	$0.313/(1 + .952A^{0.836})$	4–5	.04–.06	780	280	0.64	U: Merritts and Vincent [1989]
Tenmile	CA Coast	Sherwood Peak	greywacke	1000–2000	0.4	1.40	2.04	$0.278/(1 + .550A^{1.180})$	6–8	.04–.14	890	305	0.66	U: Merritts and Vincent [1989]
Howard	Oregon Coast	Mount Peavine	wacke	2000–2400	0.1–0.2	0.46	0.169	$0.834/(1 + 4.28A^{0.471})$	5–10	.04–.14	1097	561	0.49	O: Personious [1995]
Dry	Oregon Coast	Father Mountain	wacke	2000–2400	0.1–0.2	0.85	0.133	$0.730/(1 + 4.95A^{0.744})$	4–5	0.03	610	158	0.74	O: Personious [1995]
Big	North Carolina	Luftee Knob	ss,silt-s, m-greywacke	1200–1800	0.05–0.08	0.28	0.124	$0.880/(1 + 5.17A^{0.593})$	5–8	.03–.15	1780	1317	0.26	R: Dendy and Champion [1978]
Hurricane	Arkansas	Bidville	ss,silt-s,shale, wacke	1120–1320	0.07	0.52	0.066	$0.584/(1 + 9.61A^{0.810})$	3–5	.03–.05	683	463	0.32	R: Dendy and Champion [1978]
Knawls	West VA	Walkersville	shale,silt-s,ss,ls	1020–1300	0.01–0.03	0.70	0.029	$0.516/(1 + 16.5A^{0.670})$	1–2	.03–.04	433	311	0.28	R: Dendy and Champion [1978]
								1:50,000 Scale Maps						
Trapachillo	Ecuador	NVIII-A4	granitic	600–1300[e]	0.7–0.75	0.08	0.048	$0.948/(1 + 3.06A^{0.538})$	10–17	.04–.16	2280	1500	0.34	O: Coltorti and Ollier [2000]; E: Steinmann et al. [1999]
Jellamayo	Peru	2340–III	granitic	~500	0.3	0.40	0.601	$1.53/(1 + 2.75A^{0.455})$	15–17	.10–.40	5300	3325	0.37	E: Laubacher and Naser [1994]
Chasong-gang	N. Korea	NK-52-7-44	granite	1000–1200	0.04–0.37	0.71	0.306	$0.533/(1 + 2.28A^{0.372})$	6–10	.07–.08	1560	780	0.50	S: Yoon and Woo [2000]; E: Lim and Lee [2000]
Simbolar	Argentina	2966-9-2	migmatitic gneiss	200–300	0.18–0.28	0.47	0.47	$0.481/(1 + .479A^{0.995})$	6–15	.08–.60	3750	2925	0.22	S: Walling and Webb [1983]

Table 3. (continued)

River	Location	Quadrangle	Lithology[b]	Average Rain, mm/yr	Erosion Rate, mm/yr	m/n	$[(-dz/dt)/K]^{1/n}$	Debris Flow $a_0/(1 + a_1A^{a_2})$	Scaling Transitions Area, km²	Slope	Valley Head, m	River Head, m	Debris Flow Fraction	Erosion Rate Reference[c]
Golema	Greece	K-34-115-1	gneiss, schist, amphib.	600–800	0.22	0.57	0.179	$0.352/(1 +826A^{0.758})$	4–8	.09–.10	1600	1180	0.26	R: Poulos et al. [1996]
Marin	Kenya	76/1	qtzites, schists, gneiss	1015–1525	0.1	0.88	1.51	$0.598/(1 +616A^{0.618})$	15	.10–.27	3260	1780	0.45	O: Roessner and Strecker [1997]
Chibalan	Guatemala	2061-II	schist, gneiss, marble	1000–2000	0.04–0.09	0.73	0.794	$0.362/(1 + 1.40A^{0.953})$	9–16	.07–.20	2080	1400	0.33	S: Walling and Webb [1996]
Baay	Philippines	3172-I	basalt/and., diorite	~3500	1.4	**1.17**	**1.94**	$0.321/(1 +690A^{0.770})$	9–17	.05–.10	1600	900	0.44	R: White [1988]
Thia	Vietnam	5852 II	clastics/volcanics	2000–2400	0.08–0.50	0.32	*0.163*	$0.410/(1 +.042A^{1.720})$	17–21	.05–.11	2920	1280	0.56	E: Maluski et al. [2001], Carter et al. [2000]
Tulahuencito	Chile	D-85	clastics/volcanics	300[e]	0.4	0.41	0.205	$1.91/(1 + 12.0A^{0.383})$	7–10	.05–.14	3600	2600	0.28	O: Munoz and Charrier [1996]
Asahi	Japan	NI-53-15-4/5249 II	ss, slate, basalt, chert, ls	1600–2400	1.9–2.0	0.60	0.491	$0.678/(1 +459A^{0.691})$	12–20	.13–.17	2500	1080	0.57	R: Ando et al. [1994], Takemura et al. [1997]
St. Germain	France	27–40	mica schist	1500–2000	0.01–0.37	**0.69**	**0.151**	$0.410/(1 +853A^{2.850})$	4–5	.04–.06	960	520	0.46	R: Gay and Macaire [1999], Maneux et al. [2001]
Peinan	Taiwan	9519–II	slate, phyllite, schist	1500–3000	2–6	**0.98**	**5.63**	$0.516/(1 +201A^{0.890})$	18–80	.08–.12	3100	1300	0.58	S: Li [1976]; E: Liu et al. [2001]
Anghou[d]	Taiwan	9517-I	argillite, ss(Lushan)	3000–4000	0.4–1.7	**0.70**	**0.18**	$0.682/(1 + 2.18A^{0.591})$	4–8	.05–.08	900	240	0.73	E: Liu et al. [2001]
Ter	Spain	37–10	schist, flysch	500–1000[e]	0.07–0.13	**0.85**	**1.01**	$0.415/(1 +.070A^{2.420})$	5–18	0.10	2400	1620	0.33	R: Serrat [1999], Salas et al. [1997]; O: Verges et al. [1995]
Toplodolska	Serbia	3481 I	ss	500–1000	0.1–0.2	*0.72*	*0.638*	$0.520/(1 +.586A^{0.935})$	11	.06–.02	1880	1060	0.44	R: Pekovic et al. [1999]; S: Kostadinov and Markovic [1996]
Nam Se	Thailand	4569-I	ss/ms	1200–1400	0.01–0.09	*0.17*	*0.066*	$0.796/(1 + 4.10A^{0.772})$	6–8	.03–.14	1700	1300	0.24	R: Jantawat [1985]; S: Alford [1992]
Marrechia	Italy	278	mudstone/marls	1000–1500[e]	0.08–0.4	0.36	0.072	–	–	–	–	–	–	O: van der Muelen et al. [1999], Coltorti and Pieruccini [2000]
Djemaa	Algeria	Oued Amizour	sandstone, mudstone	1000–2000	0.1–0.26	**0.98**	**1.42**	$0.426/(1 +.371A^{1.120})$	10–20	.07–.09	1520	780	0.49	R: Errih and Bendahou [1997]; U: Morel and Meghraoui [1996]
Vistula	Poland	2917 II	flysch/marl	1000–1500	0.01–0.03	**0.68**	**0.196**	$0.590/(1 + 4.49A^{0.794})$	4–7	.05–.08	1060	740	0.30	S: Lajczak [1990]

a Bold values indicate that power law regressions have R^2 values greater than 0.9; italic values indicate R^2 values are less than 0.7.
b Lithology abbreviations are micac., micaceous; ss, sandstone; amphib., amphibolite; silt-s, siltstone; m-greywacke, meta-greywacke; ls, limestone; qtzites, quartzites; and, andesite; ms, mudstone.
c From S, suspended load; R, reservoir; E, fission track/cooling; U, marine terrace; and/or O, other.
d Field checked.
e Median annual rainfall.

Figure 4. Removal of Tyee Formation sandstone grains ($\sim$0.5–1 mm in diameter) on Sullivan 1 by abrasion caused by 1996 debris flow (see Figure 5 for location). Moss in the lee of the smaller ledge indicates abrasion of less than several mm. Ledge in bottom portion of photo corresponds to removal of fractured slab 7 mm thick.

up profile that included lower gradient sections beyond the occurrence of debris flows (e.g., slopes < 0.02). We measured area and slope along main stems, bounded at the lower end by lakes, oceans, changes in geology or reaches with slopes below 0.001 where gravel-sand transitions may lead to longitudinal profile changes [e.g., *Yatsu*, 1955]. In the United States we use 1:24,000 topography. We chose 1:50,000 scale maps for the rest of the world because they are the largest scale topographic maps available for many countries. We selected an average of five basins per continent from Europe, Africa, Asia, and South America. From North America, we selected steepland basins from the Appalachians, Oauchitas and the western United States. All of the basins we sampled are reported, including those with large amounts of local scatter in river slope. The quality of geologic and topographic data outside the United States varies greatly, so we use the global data primarily to explore the generality of a scaling break, rather than the form of the area-slope data above it. In one case (Anghou River, Taiwan), we can evaluate the accuracy of 1:50,000 data because we have 1:5,000 data for the same basin from the Taiwan Department of Forestry. Also included in Table 3 are estimates of mean annual rainfall, geology and erosion rate for each of the basins considered. The quality of these estimates varies and most should be regarded as illustrative. The last column of Table 3 lists sources for erosion rate data, many of which are from reservoir sedimentation studies or fission track data, each of which has limitations. The term "other" encompasses techniques like dating of strath terraces or sediment dating by cosmogenic radionuclides.

3. Site Description

[11] We report field and topographic evidence for bedrock incision by recent debris flows from 13 sites (Table 2) in the western United States. At three other sites, older debris flow deposits lie directly on the valley bedrock floor, indicating the possibility of a similar erosion process (last 3 sites, Table 2). In addition, we mapped the locations of the upstream-most strath terrace and the downstream-most debris flow deposits at eight basins in the western United States and Taiwan (those referred to by footnote d in Table 3), and compared this approximate process boundary to the pattern of area-slope data. Below, we report site descriptions for these localities in the order in which they are shown in Tables 2 and 3.

[12] In Oregon, intense rainfall of the 1996/1997 El Niño storms triggered landslides across the Coast Range, including Elliot State Forest near Coos Bay. Here, many landslides mobilized as debris flows (Figure 2), sweeping sediment from valley floors to expose sandstones and siltstones of the Eocene Tyee Formation (Figures 3 and 4). Erosion rates in the central Oregon Coast Range are thought to be between 0.1 and 0.2 mm/yr on the basis of strath terrace ages [*Personious*, 1995], sediment yield [*Reneau and Dietrich*, 1991] and cosmogenic radionuclides from the Coos Bay site
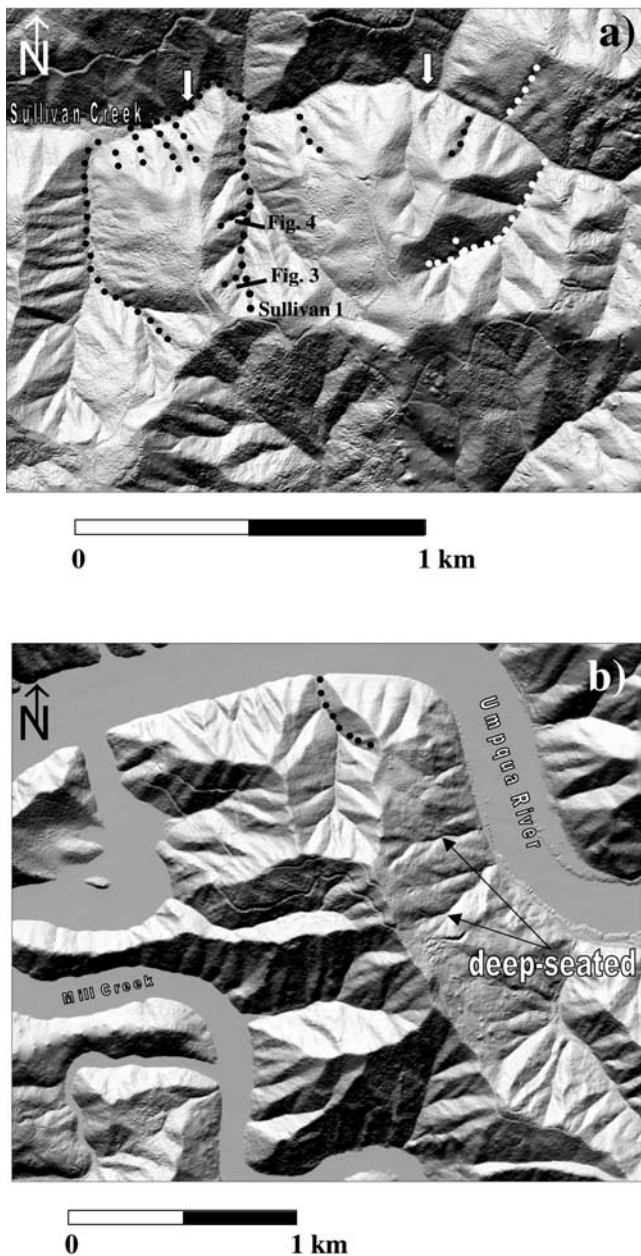
Figure 5. Shaded relief image of high-resolution airborne laser altimetry from Oregon at (a) Coos Bay and (b) Scottsburg. Dotted lines indicate 1996/1997 debris flows, as mapped in the field. Arrows in Figure 5a bracket knickpoint on Sullivan Creek. Hillslopes draining to Sullivan Creek from the top portion of the image are likely deep-seated failures (as judged by the lack of larger valleys), so we chose not to use them for analysis. Deep-seated landslides also occur in the northeast quadrant of Figure 5b, and are a process whose occurrence in this region is in part structurally controlled [*Roering et al.*, 1996].

in Figure 5a [*Heimsath et al.*, 2001]. We used ground reconnaissance and maps of debris flows provided by Oregon Department of Forestry to locate debris flow sites in or near to Elliot State Forest (numbers 1–8 in Table 2). High-resolution topography from laser altimetry covers two sites with recent debris flows (Figures 5a and 5b) near the

northern (Scottsburg) and southern (Sullivan) extremities of Elliot State Forest. Figure 5a shows a shaded relief image of Sullivan Creek in which average data spacing was 2.5 m with ∼0.3 m vertical resolution; Figure 5b shows a similar image for Scottsburg in which average data spacing was 4 m with ∼0.3 m vertical resolution.

[13] During the winter of 1996/1997, many of the prominent tributary valleys in Figure 5a experienced debris flows (dotted lines) that scoured bedrock to the main stem confluence with Sullivan Creek. We walked debris flow run outs shown in Figure 5a and mapped the occurrence and style of bedrock lowering. Although difficult to quantify systematically, we found that bedrock had been removed as (1) grooves and lineations at the scale of the component rock grains and as (2) fracture-bounded blocks one to several centimeters thick (Figures 3 and 4). We did not observe fluvial potholes, sorted sediment or strath terraces along debris flow run out paths. The remaining basins have not been scoured in the last several years, except for Sullivan 4 (just west of Figure 6a), which was largely scoured to bedrock, but was too steep to access. Figure 5b is a shaded relief image from high-resolution laser altimetry showing steeplands at the northern edge of Elliot with a 1996/1997 debris flow (dotted line) that scoured bedrock along its run out path. We also used high-resolution laser altimetry (average data spacing was 2.5 m with ∼0.3 m vertical resolution) from 1997 debris flow sites in the Tyee Formation near Roseburg (numbers 9–11 in Table 2), which we do not show for space reasons.

[14] In Utah we visited valleys scoured by debris flows along the Wasatch front, whose long-term erosion rates in the vicinity of the Salt Lake City segment are of order 1–2 mm/yr on the basis of fission track and U/Th-He data [*Armstrong et al.*, 1999]. Just north of Salt Lake City in Paleozoic gneiss of the Farmington canyon complex, we walked the lower reaches of two valleys (Steed and Rick's Ford, numbers 14–15 in Table 2) scoured to their fans by debris flows in the early part of the century [*Wooley*, 1946]. These have largely been refilled with bouldery debris, and bedrock is exposed only at a few waterfalls. Adjoining basins that were scoured to bedrock during 1982 debris flows [*Williams and Lowe*, 1990] also have only rare exposures of bedrock. Further south, we walked the run out of a 1997 debris flow (Joe's Canyon, number 13 in Table 2) that scoured the Mesozoic Oquirrh Formation, a quartzite in the foothills of the Wasatch near Spanish Forks. There we observed decimeter-sized blocks missing from the jointed quartzite bedrock of the valley bed, which also had ubiquitous abrasion marks like those in the Tyee Formation (Figure 4). When we walked the channel it was dry, and lacked exposures of sorted sediment, well defined channel banks and fluvial features like potholes or plunge-pools.

[15] In the San Bernardino Mountains a 1999 debris flow scoured schists of the Yucaipa Ridge (number 12 in Table 2), before depositing in Valley of the Falls. Here, long-term erosion rates are estimated to be around 1 mm/yr from U/Th-He data [*Spotila et al.*, 1999]. Along the run out, we observed abrasion and block-plucking of the bedrock valley floor caused by the debris flow, which also removed a preexisting talus cover at valley slopes mostly above 0.10.
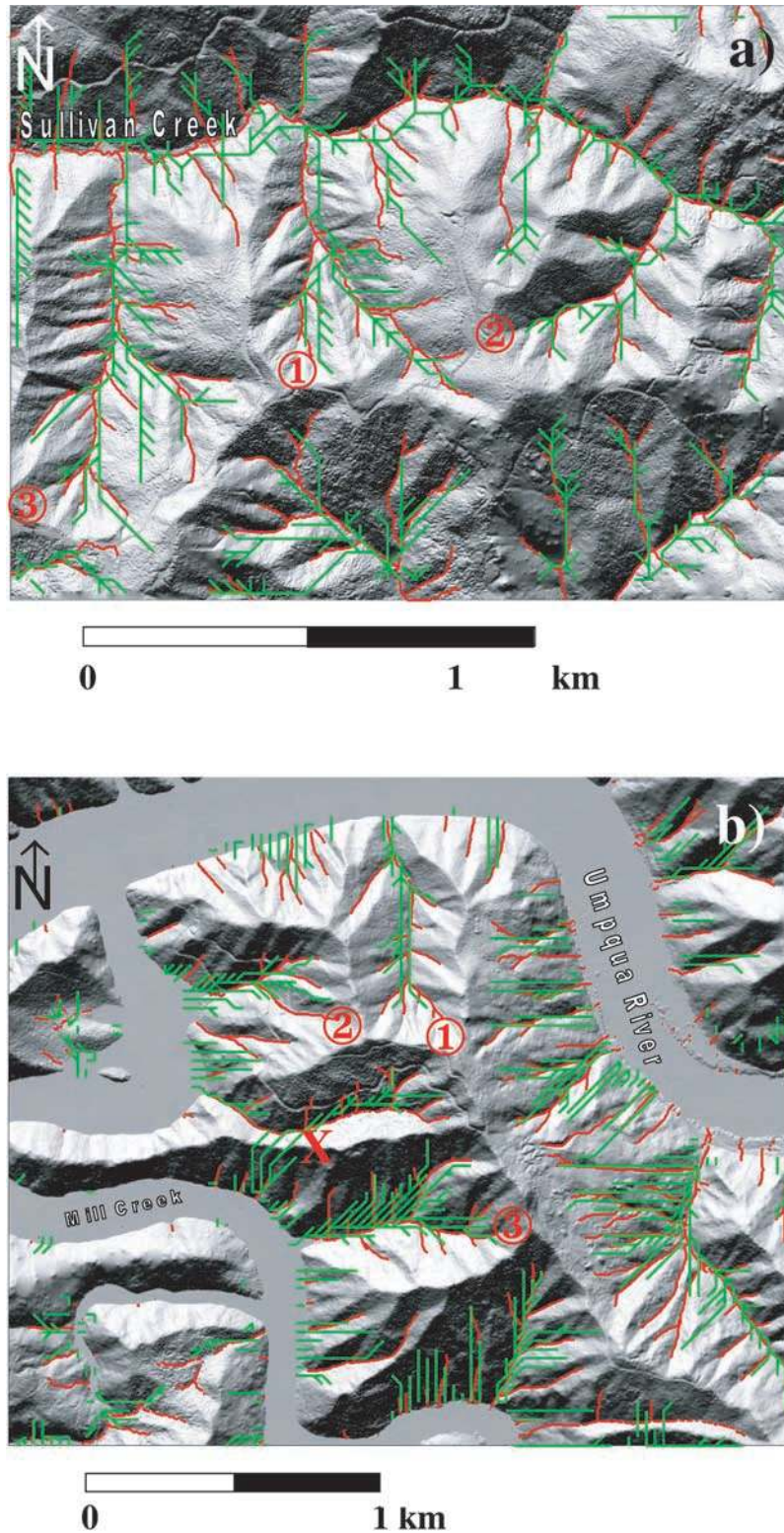
Figure 6. Valley networks with drainage areas greater than 4500 m^2 using laser altimetry (red) and USGS 30-m grids (green) at (a) Coos Bay and (b) Scottsburg. Profiles were selected to avoid regions with deep-seated failures. The 30-m data poorly represents the valley network because it results in many artifactual valleys located on hillslopes and has spurious valleys like that crossing a ridge in Scottsburg (center left, cross symbol). Numbers refer to drainage basins used for area-slope analysis.

[16] We visited a basalt basin (Aa, number 16 in Table 2) in East Maui and mapped debris flow deposits to its confluence with the main stem Iao Valley. Bedrock near the junction was largely buried with diamicton, and only exposed in a roadcut.

[17] Bear River in the San Gabriels cuts Mesozoic granodiorites at long-term erosion rates of ~1 mm/yr [*Blythe et al.*, 2000]. Its headwater valley is filled with coarse talus, and several debris flows occurred in its tributaries the day before we visited, running out to slopes of 0.11 (Table 1). Below these recent debris flow deposits, boulder fields fill the valley for several hundred meters until the first widespread bedrock exposure occurs with potholes and runnels.

[18] In the Santa Cruz Mountains, Deer Creek (Table 3) cuts Neogene arkoses at rates that range from 0.2–0.3 mm/yr, as estimated from sediment yield [*Brown*, 1973] and cosmogenic radionuclide analysis of sediment [*Perg et al.*, 2000]. The headwaters of this valley are filled with coarse colluvium with rare exposures of sandstone cliffs. At around 0.10 valley slope we found a field of boulder berms containing auto tires from historic debris flows. Downstream of these recent deposits we found cascades of boulders and isolated patches of older diamicton. Strath terraces begin further downstream in pool-riffle reaches.

[19] Honeydew, Elder and Noyo rivers in the northern California Coast Range cut Mesozoic greywackes of the Franciscan Formation and strath terraces are common up to slopes of ~0.05. Projection of marine terrace rock uplift rates from *Merritts and Vincent* [1989] inland to these basins yields approximate rock uplift rates of 4.0, 0.7, and 0.4 mm/yr, respectively. Headwater reaches in these valleys share the features of Deer Creek, although deep-seated failures occur in the Noyo basin.

[20] Finally, Anghou River drains the Eastern side of Taiwan, cutting sand- and siltstones of the Miocene Lushan Formation at rates estimated to be 1–2 mm/yr by fission track analysis [*Liu et al.*, 2001]. Its downstream braided reaches transition to step-pool bed forms near the end of recent debris flow boulder berms.

4. Methods

[21] The handwork involved in collecting area and slope from paper contour maps is labor intensive and slow. We tested the possibility that we could extract similar data quickly from 30-m USGS DEMs by comparing them to hand-collected data from their source 1:24,000 maps, and to laser altimetry in Figure 5b. We used a common threshold drainage area of 4500 m^2 (five 30-m grid cells) to extract a valley network from DEMs, and looked for mismatches in the network position, and resulting area-slope graphs.

[22] Figure 6 reveals substantial errors in both the position and extent of the network as estimated from the USGS 30-m DEM in green, compared to laser altimetry in red. The upper branches of the 30-m network are largely artifacts (e.g., feathering [see *Montgomery and Foufoula-Georgiou*, 1993]), and include portions of hillslopes rather than just valley floors (which are commonly between 3 and 6 m width). In some places, the 30-m valleys are entirely artifacts, like the valley in the center left panel of Figure 6b that cuts through a ridge (marked as a cross). In addition, 30-m DEMs poorly resolve small valleys compared to the original 1:24,000 contour maps. For instance, Figure 7

compares hand-measured area-slope data with 30-m DEM data for a steep basin in the King Range, California. We removed sinks from the source 30-m data by increasing the elevation of such cells in 0.1 m increments. We extracted the valley network with a threshold drainage area of 5 or more cells, and removed cells that were influenced by sinks. Although the derivative 30-m data are similar to the contour data in some respects (m/n values are almost within one standard error), the scatter of the 30-m data obscures the region in which the data change trend. It is this region that defines the extent of fluvial power law relations, and therefore 30-m data are not adequate to resolve this issue. Although averaging by log-binning smoothes noise, it does not recreate the original data pattern.

4.1. Techniques for Hand Extraction of Area-Slope Data

[23] We conclude that network extraction from 30-m DEMs in steeplands where valley bottoms are substantially less than 30 m wide introduces noise to the source data. Therefore, except for the laser altimetry, we measured main stem valley area and slope by hand from contoured 1:24,000 or 1:50,000 scale topographic maps. To make area-slope plots for valleys in the laser altimetry coverage, we extracted the valley network using a simple threshold drainage area of 1000 m^2, which approximates the valley network that we observe in the field here. We used a maximum fall algorithm for slope with a forward difference of two grid cells, extracted the profile data, and binned and averaged values over 10-m increments to smooth slope variations from thick-bedded sandstone cliffs. For all other sites we measured slope and drainage area at a point equidistant between elevation contours for every contour crossing of the valley. We enlarged steep areas with closely spaced contours 200% on a photocopier. Where contours are closely spaced, we sampled area at every other contour interval, measuring slope between adjacent contours. We calculated slope as the contour interval divided by the valley blue-line distance, or if these are absent, the shortest distance along valley between adjacent contours. We stopped collecting data near the drainage divide at the valley head, which we defined as the last segment where the contour direction angle from one side of the valley to the opposite changes by ~150° or less. This is a crude approximation for the actual hollow location, but we found it to be a rough measure of valley head location based on comparison of 1:24,000 maps to field observations of hollows in Figure 5. We used a polar planimeter to measure drainage area, resulting in a precision of ±0.001 square inches (e.g., 3.7×10^{-4} km^2 for 1:24,000 maps). Using a ruler to measure horizontal distance between contours results in a precision of ±0.25 mm (6 m for 1:24,000 maps, 3 m for the 200% enlargement). Corresponding point uncertainties in slope range from small fractions of a percent in the lowlands to 50% in the steepest parts of the profile, although practical uncertainties appear less than 20% on the basis of field and laser altimetry comparison to contour maps.

4.2. Techniques to Extract Power Law Portion of Data

[24] We used three methods to identify potential fluvial power law segments of main stem area-slope plots. All three assumed that valleys carved by fluvial processes have area-slope data fit best by a power law, although we recognize
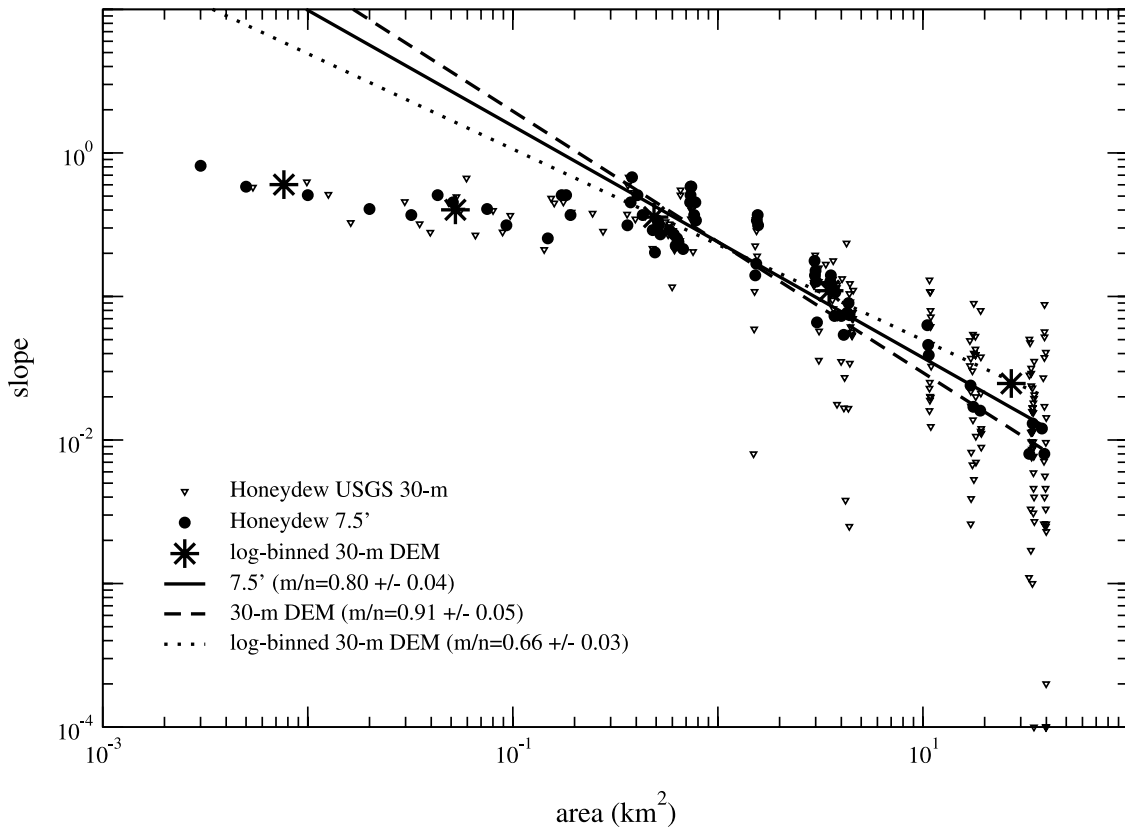
Figure 7. Comparison of USGS 30-m grid and hand extracted 1:24,000 data for Honeydew valley in the King Range, California. Sinks and adjacent points are omitted from profile, slopes calculated using forward difference, maximum fall algorithm over 2 cells. Scatter of 30-m data compared to its 1:24,000 source data indicate derivation errors leading to differences in slope and intercepts of power law regressions (shown for data below apparent scaling break at ~0.4 km^2). Binning the data by log cycle and averaging it further alters the slope of the source data and obscures its curvature.

that systematic variations in lithology, rock uplift rate [*Kirby and Whipple*, 2001], sediment supply [*Sklar and Dietrich*, 1998; *Sklar and Dietrich*, 2001], orography [*Roe et al.*, 2002] or grain size can influence this pattern. Although we assume that power laws approximate the lower portions of valley profiles, we are not able to demonstrate this over more than 2–3 log cycles because the gravel bedded rivers that we examine are commonly bounded by dams, oceans or the gravel-sand transition at 0.001 slope. Many of the data that we present have substantial scatter when compared to area-slope plots often presented in the literature because we do not smooth data by averaging it.

[25] Our first two methods used successive pruning of data starting at the top of the profile and proceeding down valley until a specific criteria for linearity was met. For instance, in the first method we fit a power law to all of the data and recorded its slope. We then pruned the smallest drainage area data point and refit the power law to get a new slope. When this process is repeated, regression slopes tend to increase as successively larger drainage areas are removed, indicating that the data do not follow a single power law. We found that regression slopes stopped increasing systematically where the remaining data included only low valley slopes and large drainage areas, consistent with a power law in the fluvial region. A complementary method

used the same pruning procedure but fit log-log quadratic curves to data until the t statistic of the quadratic term was judged to be negligible and remaining data were well represented by a single power law.

[26] A third approach is to fit a function to the data which approaches valley head slopes (s_0) at small drainage area, and curves toward a linear power law scaling ($a_1 A^{a_2}$) at large drainage area:

$$S = \frac{s_0}{(1 + a_1 A^{a_2})} \qquad (5)$$

Equation (5) provides an empirical fit to the curved debris flow valley data with a minimum number of parameters. In it, s_0 represents the slope at the valley head, a_1 is inversely proportional to curvature [and has units $1/(\text{length}^2)^{a2}$], and a_2 tends toward a power law slope at large drainage areas. The second derivative of (5) can be written:

$$f''(A) = s_0 \frac{\left[2(a_1 a_2 A^{a_2-1})^2 - a_1 a_2 (a_2 - 1) A^{a_2-2} (1 + a_1 A^{a_2}) \right]}{(1 + a_1 A^{a_2})^3} \qquad (6)$$

which has units of $1/\text{length}^4$. We infer that data follow a power law in the region of the plot where this second derivative has a marginally small value (marginal curvature
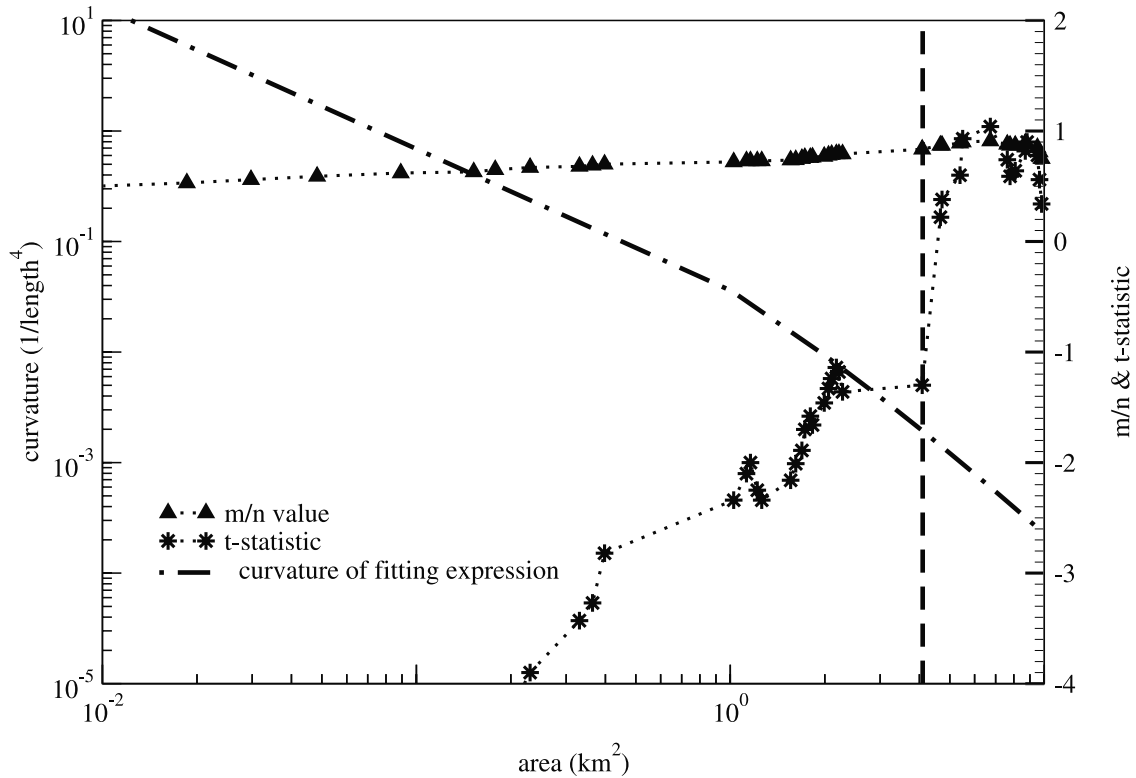
Figure 8.   Plot of three methods to extract power law portion of area-slope plot for Deer Creek (see text). The m/n value is the slope of a power law regression applied to the data when successively larger drainage areas are pruned away for each fit. Values converge when there is no systematic curvature in the data, so that it approximates a single power law. The t statistic is a measure of the significance of a quadratic term in a nonlinear fit to the data using the same pruning. It falls to negligible magnitude (below 1) where m/n values converge (vertical dashed line) and where the curvature of equation (5) reaches 10^{-3}. Together, these criteria indicate that Deer Creek has a single power law at drainage areas larger than $\sim$4 km^2.

technique) for parameter values from the fit to the full data set.

[27] The first two methods have the disadvantage that endpoints (particularly those that are downstream) exert a tremendous leverage on both m/n values in equation (4) and quadratic curvature. Even small deviations from linearity on a single downstream end point can lead to transition slope values well downstream of debris flow run outs (e.g., <0.02). Therefore these methods can only be applied to data that follow a power law exceedingly well. The third method has the advantage of being very robust to scatter in data, but requires a judgment of the threshold curvature at which the function is well approximated by a line. Therefore we use a combination of these three techniques. We used m/n and t statistics on data sets with well-defined linear portions as judged by R^2 values greater than 0.9 (bold m/n values in Table 3). Where m/n stopped increasing monotonically and the t statistic indicated that there was little significance to a quadratic fit parameter (|t| < 1), we inferred a single power law. We then used these results to choose a curvature value at which the second derivative of equation (5) was judged to be vanishingly small, so that the remaining data approximate a power law. We call the upstream-most data point on the power law the river valley head.

[28] For instance, Figure 8 shows all three methods applied to Deer Creek, for data spanning its headwaters to

near the mouth of the main stem San Lorenzo at the Pacific Ocean (Figure 1b). The m/n value stops increasing systematically where the t statistic approaches −1 at a drainage area of $\sim$4 km^2. The third line indicates curvature derived from a Levenberg-Marquardt nonlinear fit to the data using equation (5) with inverse slope weighting. Curvature values of $\sim$10^{-3} correspond to the transition to linearity as judged by the previous two techniques. We fit (5) to each full data set, and where its second derivative reaches 10^{-3} we infer the beginning of a single power law. To characterize the curvature of the data above the power law, we refit (5) to data above the threshold curvature value. For both fits, we weight each data point by the inverse of its slope, which is equivalent to weighting each data point by the valley length over which its slope is evaluated. Thus the more frequent data from steeper portions of the profile have proportionally less weight and do not bias the fit. This is comparable to weighting each DEM pixel equally along a profile, and reduces the influence of knickpoints or other short-length scale features on the fit.

5. Results

5.1. Curvature of Area-Slope Data

[29] In steepland valleys of the western United States we have observed sediment removal and bedrock lowering along the entire run out of 13 recent debris flows in Oregon,
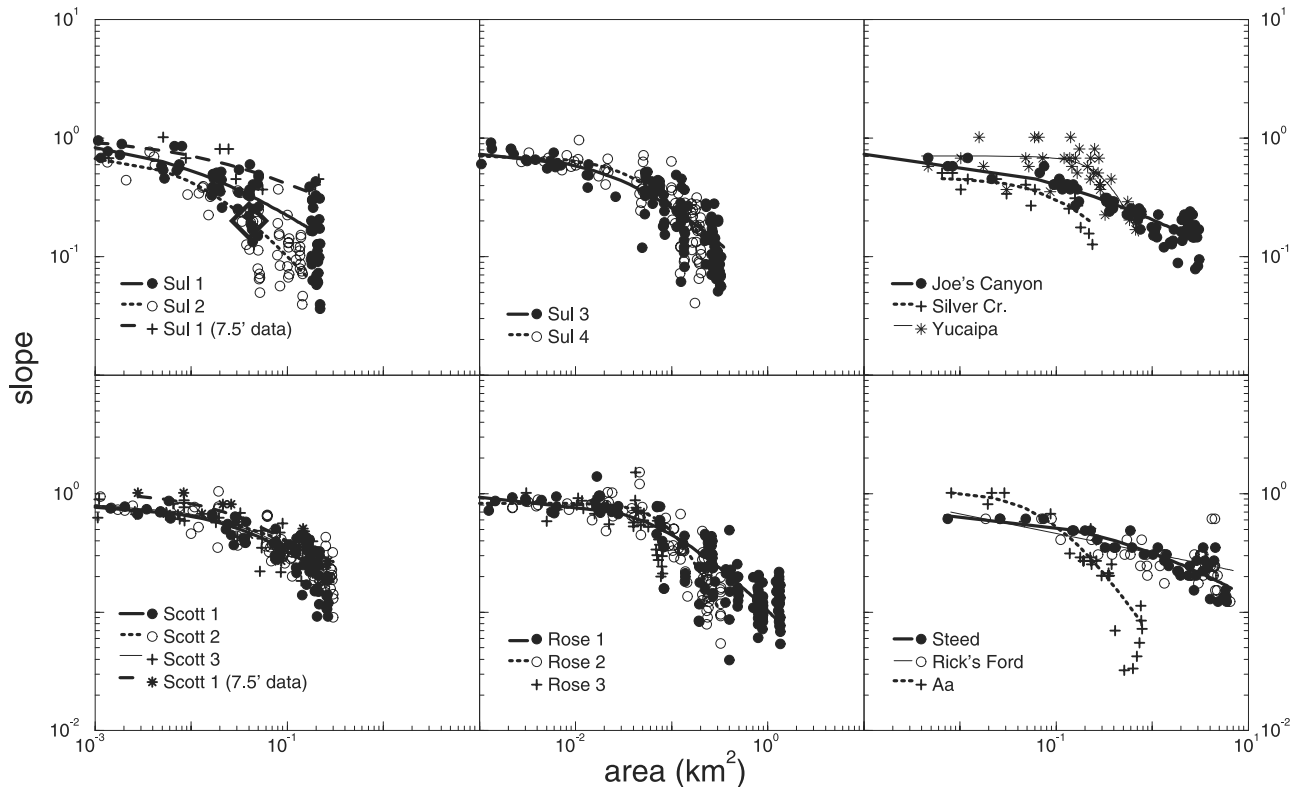
Figure 9. Area-slope data from valleys in Oregon, Utah, and California where we mapped bedrock lowering of the valley floor along the runout path of recent debris flows. Curvature in area-slope space along this runout path appears to be a signature for valley incision by debris flows. Data from Sullivan Creek, Scottsburg, and Roseburg are from high-resolution laser altimetry in Oregon; Joe's Canyon, Marlow 1, Silver Creek, and Yucaipa data are from 1:24,000 topography in Oregon, Utah, and California. A diamond in the top left panel identifies the approximate location of bedrock lowering shown in Figure 4. Also shown are data from 1:24,000 maps for basins with historic debris flow activity along their entire profile (Steed and Rick's Ford in Utah, and Aa in Maui). See Table 2 for fit parameters.

California and Utah (Table 2 and Figures 2–4). The lithologies, long-term erosion rates and climatic histories of these field sites are diverse (Table 2), yet all share evidence for bedrock lowering by block-plucking and grain-scale scour during the debris flow. These features are illustrated for Oregon field sites in Figures 3 and 4, and we have observed them where debris flows cross quartzites in Utah (number 13 in Table 2) and schists in southern California (number 12 in Table 2). Area-slope data from along all of these scoured run out paths appear nonlinear in log-log space (Figure 9) and cannot be fit with a single power law without nonrandom residuals. Area-slope data from basins with historic or prehistoric debris flows to their terminuses in Utah and Maui are also curved, although in these basins bedrock exposure along the old run out path is rare. This is consistent with rapid mantling of the bedrock surface by coarse colluvium following exposure by the debris flow. Valleys in Figure 5a that were scoured to bedrock in 1997 by debris flows were largely infilled with colluvium or vegetation when we revisited them in 2001. Although each data set in Figure 9 could be decomposed into an arbitrary number of linear segments, these would not correspond to any process transition that we observed while walking these profiles.

[30] Laser data sets in Figure 9 have substantially denser data spacing than 1:24,000 contour data, and show greater scatter, despite averaging to 10-m increments. Although the coarser 1:24,000 data capture area-slope curvature seen in laser altimetry, they do not replicate its exact form. For instance, basin number 1 has higher curvature in the laser altimetry than the 1:24,000 data, leading to different a_1 and a_2 values in Table 2. Basin number 5, by contrast, has similar curvature values, but a higher valley head slope in the 1:24,000 data. Some of the basins have curves that are largely indistinguishable from each other (e.g., Scottsburg numbers 5, 6 and 7). Amongst the rest there is substantial variation in the shape of the curvature, sometimes between adjacent basins (e.g., Sullivan and Roseburg). Variations in lithology, catchment size and transient conditions are all possible sources for different curve shapes. For instance, curvature sometimes decreases as catchment size increases (e.g., number 4 versus number 3; number 9 versus number 10) and sandstone cliffs are more frequent in some catchments (e.g., number 1).

5.2. Scaling Break at ∼0.10 Slope

[31] Along eight valleys in the western United States and Taiwan we walked from the valley headwaters past the downstream-most debris flow deposits into fluvial reaches. We found that the lowermost main stem debris flow deposits terminate at 0.04–0.12 slope, and strath terraces (if they occurred) began several hundred meters
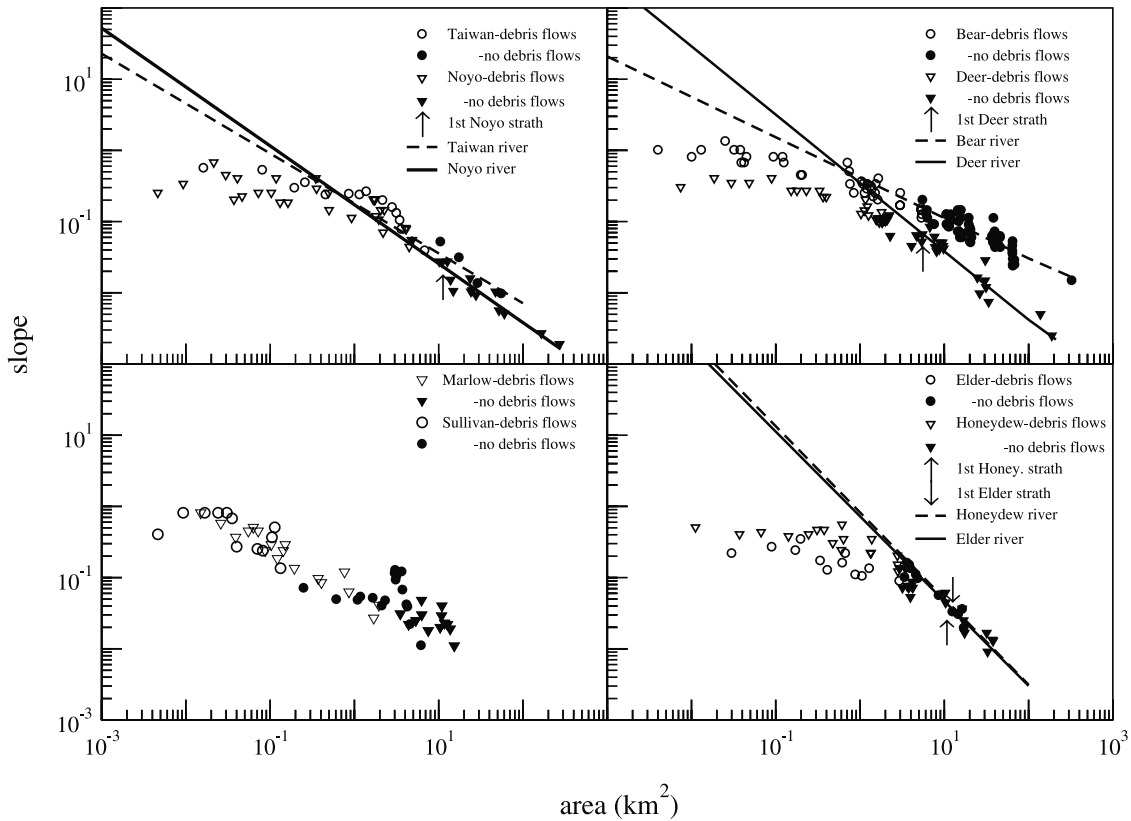
Figure 10. The extent of debris flows along the main stem as estimated by preserved deposits (open symbols) mapped in the field onto 1:24,000 topography. The zone of departure from the fluvial power law lies near the downstream end of existing debris flow deposits and upstream from last observed strath terrace. Extension of single power law (shown by lines) substantially overestimates valley slope at low drainage areas (see text for methods used to define linear portion of data). Data for each basin is bounded at its downstream end by presence of the ocean (Noyo, Taiwan, Deer, Honeydew, Marlow, and Sullivan) or dams (Bear). Sullivan and Marlow Creeks lack defined power law scaling because of a combination of knickpoints and small drainage areas. They illustrate the importance of using sufficiently large basins to define fluvial trends.

down valley from these deposits (Figure 10). Area-slope data up valley from these mapped terminal debris flow deposits (open symbols) are curved in the same manner as data from basins where we recorded bedrock scour from debris flows (e.g., Figure 9). For instance, Figure 11b shows residuals from two power law fits to Deer Creek shown in Figure 11a, the entire data set and a subset of slopes greater than 0.10 (location of recent debris flow deposits). For both fits, positive residuals occupy the middle of the plot, negative residuals the ends. Neither the whole plot, nor the steep portion where we have mapped modern debris flows can be fit with a single power law.

[32] Valley slopes downstream of the first strath terrace approximate a linear power law (solid symbols) as judged by a marginal curvature technique. For instance, strath terraces in Deer, Noyo, Honeydew and Elder Creeks map downstream of the beginning of the power law. In Bear, straths are absent, but the beginning of the power law region corresponds to the appearance of large potholes and runnels in the granite-floored channel. The extension of power law scaling above this transition region substantially over-predicts valley slope at low drainage areas (Figure 10) and is

therefore a poor approximation for steeper valley slopes. Marlow and Sullivan Creek basins are smaller than our other examples and may not have enough data to define a power law, particularly with knickpoints that obscure potential trends. Curvature for these basins is lower than higher-resolution laser altimetry indicates for adjoining basins, but still present in 1:24,000 data.

[33] Above the end of the power law and the upstream-most strath terraces of the valleys in Figure 10, we observed evidence that reaches transition from fluvial to debris flow activity over several hundred meters or more. In them, we observed fluvial bed forms (commonly step-pools) and fill terraces, but also occasional debris flow deposits. In Anghou, Deer, Honeydew, Elder and Bear, step-pools and rare debris flow deposits of the transition reaches gave way upstream to boulder cascades that filled the valley. In some basins, the slopes of these transition reaches are smaller than those found further downstream (e.g., Noyo, Deer, and Honeydew basins) but increase rapidly upstream once debris flow deposits become common. Valleys upstream of the transition region are straight or broadly curved in planform, but lack the repetitive meandering seen in rivers. If present, fill terraces were commonly bouldery debris flow
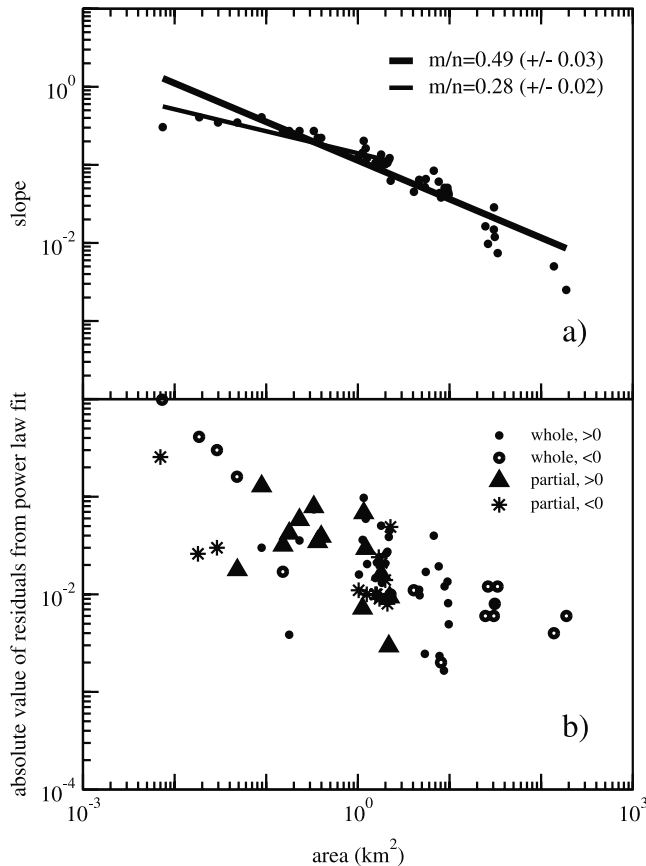
Figure 11. (a) Plot of Deer Creek, Santa Cruz Mountains. Extension of a fluvial power law to steep valleys is inappropriate, as shown by nonrandom residuals. Also note that the trend at small drainage areas is nonlinear. Catchment bedrock is sandstone, erosion rates are 0.15–0.3 mm/yr (see text for details). (b) Absolute values of differences between predicted and observed slopes in Figure 11a show a nonrandom pattern indicating that only the lower fluvial section is linear.

deposits that had been partially incised. Bedrock exposures along the valley floor were restricted to a few waterfalls.

5.3. Extension to Other Steeplands

[34] The scaling break that we observe in Figure 10 also occurs in steepland basins in the United States (Figure 12a) and around the unglaciated world (Figure 12b). At larger drainage areas, the slopes of many of these basins approximate a power law (e.g., Djemaa, Vistula, Golema, Deer, Noyo, Bear, Indian and Honeydew basins). Although there is significant scatter in some of the basins (e.g., Nam Se, Trapachillo, Simbolar), projection of power laws to small drainage areas would not predict valley head slopes substantially in most cases (e.g., Figure 10). The sole exception is a mudstone basin from Italy (Marecchia) that may have badlands dominated by overland flow in its headwaters (M. Casedei, UCB Earth and Planetary Science, personal communication, 2002).

[35] We extracted the power law portion of the data for most of the basins in Figure 12 (except Marecchia, Marlow and Sullivan) using marginal curvature techniques with equation (6) and then fit nonlinear data up valley (usually including transition reaches discussed above) with equation (5). Table 3 summarizes parameters from fluvial power law fits including the slope (m/n) and intercept $\{[(-\partial z/\partial t)/K]^{1/n}\}$, as well as parameters from the fit of equation (5) to data above the power law region. Also shown are the approximate slopes and drainage areas at the transition, elevations of valley and river valley heads on the source contour map, and the fraction of valley relief within the debris flow region.

[36] This fraction is defined as elevation difference between valley head and scaling transition point (river head) divided by the elevation of drainage divide. We used the last drainage area in the debris flow region, and the first in the power law region to bracket the drainage area of the scaling transition. We estimated the slope values at the transition by using the lowest debris flow slopes and the highest river slopes around the transition. Where rivers have locally steep slopes (e.g., Simbolar, Jellamayo) or debris flows have locally low slopes (e.g., Knawls, Indian), these values are included, leading to substantial ranges.

[37] We found that valley slopes begin to fall systematically below the fluvial power law prediction as they approach values from 0.03–0.10 (see scaling transitions column in Table 3), similar to results from Figure 10. Just above the river head, there is commonly a short region where slope increases more rapidly than anywhere else on the plot (e.g., Honeydew, Deer, Djemaa, Nam Se, St. Germain, Ter, and Simbolar). This occurs where the curved data do not join the power law fluvial trend asymptotically. Above this high curvature region, there is commonly a more gentle curvature as the valley head is approached. The magnitude of curvature (approximated by a_1 in Table 3) varies widely among basins. Grouping the basins by map scale, and by lithology and erosion rate can reduce the variation. For instance, for the last 12 U.S. basins dominated by sedimentary rocks in Table 3, a plot of erosion rate against a_1 in log-log space shows a rough correlation ($R^2 = 0.77$) with curvature increasing with erosion rate. Global data in basins of sedimentary rock (excluding the Marecchia and basins with combinations of clastics and metamorphic rocks) show a similar relation, although they are more scattered ($R^2 = 0.70$). Basins with crystalline rocks on the other hand tend to have lower curvature for similar erosion rates. For instance, at erosion rates between 0.1–0.3 mm/yr, Djemaa and Toplodolska basins cut in sedimentary rocks have lower a_1 values (thus higher curvature) than Simbolar, Chasong-gang and Jellamayo basins, which are cut in granites and gneisses. Because a_1 trends with erosion rate and lithology are weak enough to be challenged, and the erosion rates for many of the basins have large but unquantifiable uncertainties, a more focused effort is required to evaluate these correlations with lithology and erosion rate.

[38] Figure 12 and s_0 values in Table 3 illustrate that these valleys heads approach slopes of 0.3–1, and more commonly slopes of 0.4–0.5, over a wide range of lithology and erosion rates. Comparison of 1:50,000 to 1:5,000 data for the same basin (upper-left panel in Figure 12b) indicate that coarser topography captures a smoothed version of finer-resolution data, so curvature from 1:50,000 scale maps is not an artifact of coarse scale.
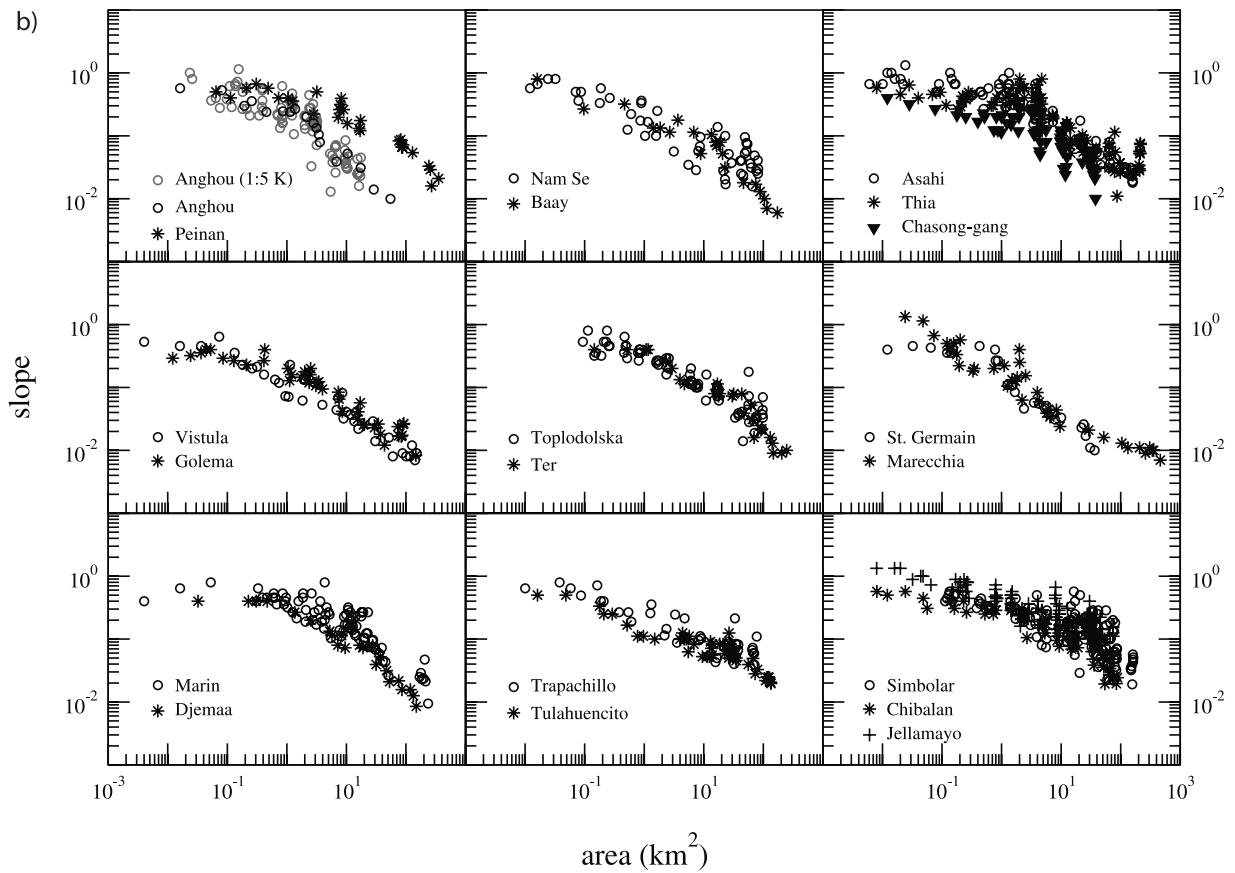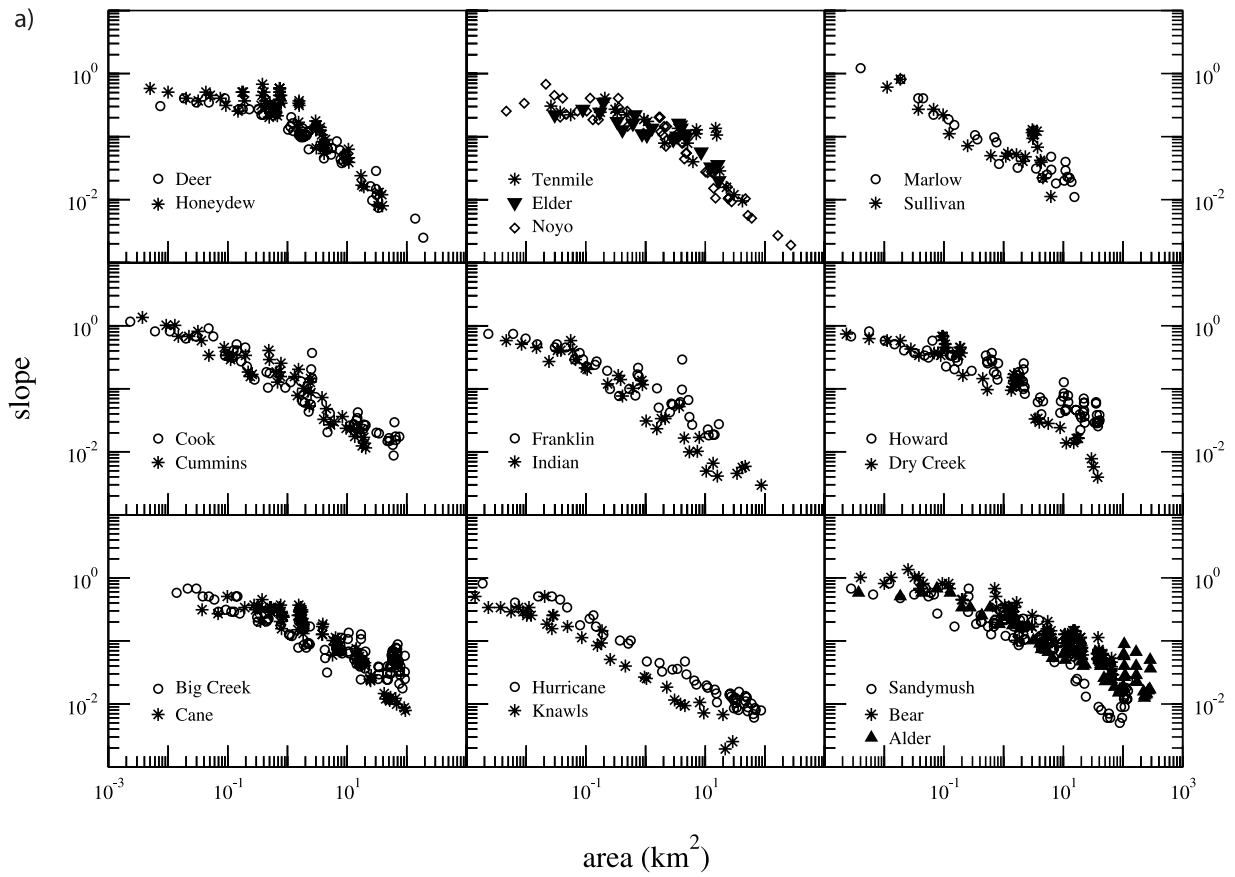
[39] Below the scaling break, the exponents of the power law regression vary substantially, from near zero values to 1.4 (Table 3). Basins with power law fits whose R^2 is greater than 0.9 are shown in bold, and those with R^2 less than 0.7 are italicized. The former have m/n values from ~0.7 to 1.0 for sedimentary and metamorphic lithologies. Basins with intermediate R^2 values have a greater range of m/n, from ~0.5–1.4. Many low R^2 values result from local, steep down valley reaches that disrupt a power law trend (e.g., Big Creek, Sandymush and Toplodolska) or pervasive scatter so that linear trends are less obvious (e.g., Nam Se, Simbolar, Jellamayo, and Trapachillo). Power laws fits to the latter basins have low slopes whose upstream projections intersect data above the river valley head, but do so in regions where data actually curve.

6. Discussion

[40] Four categories of observations indicate that debris flows carve the bedrock of some steepland valleys, producing a distinctive area-slope topographic signature: (1) field observations of bedrock lowering caused by debris flows, (2) area-slope curvature in valleys with observed debris flow bedrock lowering, (3) scaling break near terminal debris flow deposits, up valley from straths (if they occur), and (4) scaling break in U.S. and global data near typical debris flow run out slopes of ~0.03–0.10.

[41] First, field observation along recent debris flow run outs indicates that where bedrock is exposed, there is evidence for lowering caused by the debris flow. The lowering is of sufficient magnitude to be geomorphically relevant (e.g., Figure 4), although its style varies with lithology. Debris flows appear to be the dominant process exposing bedrock in steepland valleys whose floors are often mantled with very coarse particles. Headwater valleys that have not had recent debris flows (e.g., those in Figure 10) lack or have only rare exposures of bedrock above step-pool reaches in slope ranges where debris flows occur. The rapid mantling of valleys in Oregon that were scoured to bedrock in 1997 also indicates that debris flows here may be the only process capable of transporting away coarse material that accumulates rapidly in valley bottoms from hillslope processes. Although sediment in valleys in Figures 2 and 3 may eventually acquire a thin veneer of fluvially sorted sediment, it is usually colluvium below the surface [see also *Benda*, 1990; *Benda and Dunne*, 1997]. Transport of colluvium by concentrated flow following debris flows is also reported [*Larsson*, 1982], but we know of no evidence for bedrock lowering by concentrated flow following debris flows. Although fluvial incision may be possible in this kind of circumstance, debris flows appear to be required just to expose most of the valley floor bedrock.

[42] Second, valleys where we have mapped scour (e.g., Figures 5a and 5b) have area-slope plots that curve in log-log space (Figure 9) throughout the overlapping regions of observed bedrock lowering and debris flow run out. Although there is much local scatter in high-resolution Oregon slope data due to alternation between sandstone and siltstone beds, linear power laws will not fit the high-resolution topography of these valleys. This curvature is also apparent on coarser-resolution data (e.g., 1:24,000 data in Figure 9), although we suspect that its exact parameterization requires higher-resolution data because Marlow and Sullivan Creek plots (Figure 9) show different curvature. We propose that although the valley networks shown in Figures 2 and 5 closely resemble fluvial networks in planform, they are predominately carved by the entirely different process of debris flow incision, whose signature is curvature in log A-log S space.

[43] Third, we find that a scaling break in the 1:24,000 area-slope data occurs approximately where identifiable debris flow deposits end and strath terraces begin (e.g., Figure 10). This transition in process is mirrored in the topography as a scaling break in valley area-slope data when plotted in log-log space. We interpret the region between frequent debris flow deposits and the beginning of strath terraces as a transition between fluvial bedrock incision and debris flow incision. Although these reaches are likely a combination of processes, we include their few data points in the debris flow region because their up valley extent is difficult to estimate.

[44] Fourth, analysis of many unglaciated steepland valleys in the United States and around the world indicates a scaling break from data that could be modeled with a single power law to data that are nonlinear in log-log space (Table 3) near where field observations (e.g., Tables 1 and 2) indicate that debris flows deposit (slopes > 0.03). Since many rivers lack strath terraces (e.g., Bear River), there are substantial uncertainties in the long-term boundary between fluvial and debris flow valley incision. Therefore the transition boundaries listed in Table 3 for valleys that we have not walked should be regarded as illustrative rather than definitive.

[45] Transient changes in valley long profile or systematic variations in rock uplift rate [*Kirby and Whipple*, 2001] or lithology may also have their own signature on area-slope plots. We have tried to minimize these effects by careful site selection, but we cannot demonstrate that all of our sites have topography at steady state. Some are likely to be out of equilibrium at some time or space scale. For instance, basins whose data are poorly fit with power laws in fluvial regions (e.g., Nam Se, Simbolar, Jellamayo, and Trapachillo) may have transient knickpoints that lower m/n values. Although fluvial power laws do not overestimate some slopes above river valley heads in these basins, they also do not capture curvature above the river valley head. What we find convincing is that across a wide range of rock uplift rates and lithologies, the scaling break takes place at around 0.03–0.10, the lowest slopes that many field studies indicate that larger debris flows can reach (e.g., Table 1).

[46] While the evidence that we have acquired points toward the dominant role that debris flows play cutting steepland valleys, it does not mean that all valleys greater than 0.03–0.10 slope are cut solely by debris flows. In landscapes without mass failures (e.g., some badlands), overland flow may still predominate. Nor have we estab-

---

Figure 12. (opposite) Data from unglaciated steepland valleys (a) in the United States (1:24,000) and (b) around the world (1:50,000). Note that extension of linear power law trends of large drainage areas would tend to overpredict valley slope above 0.10 across a wide range of climate, rock uplift rates, and lithology. See Table 3 for details.
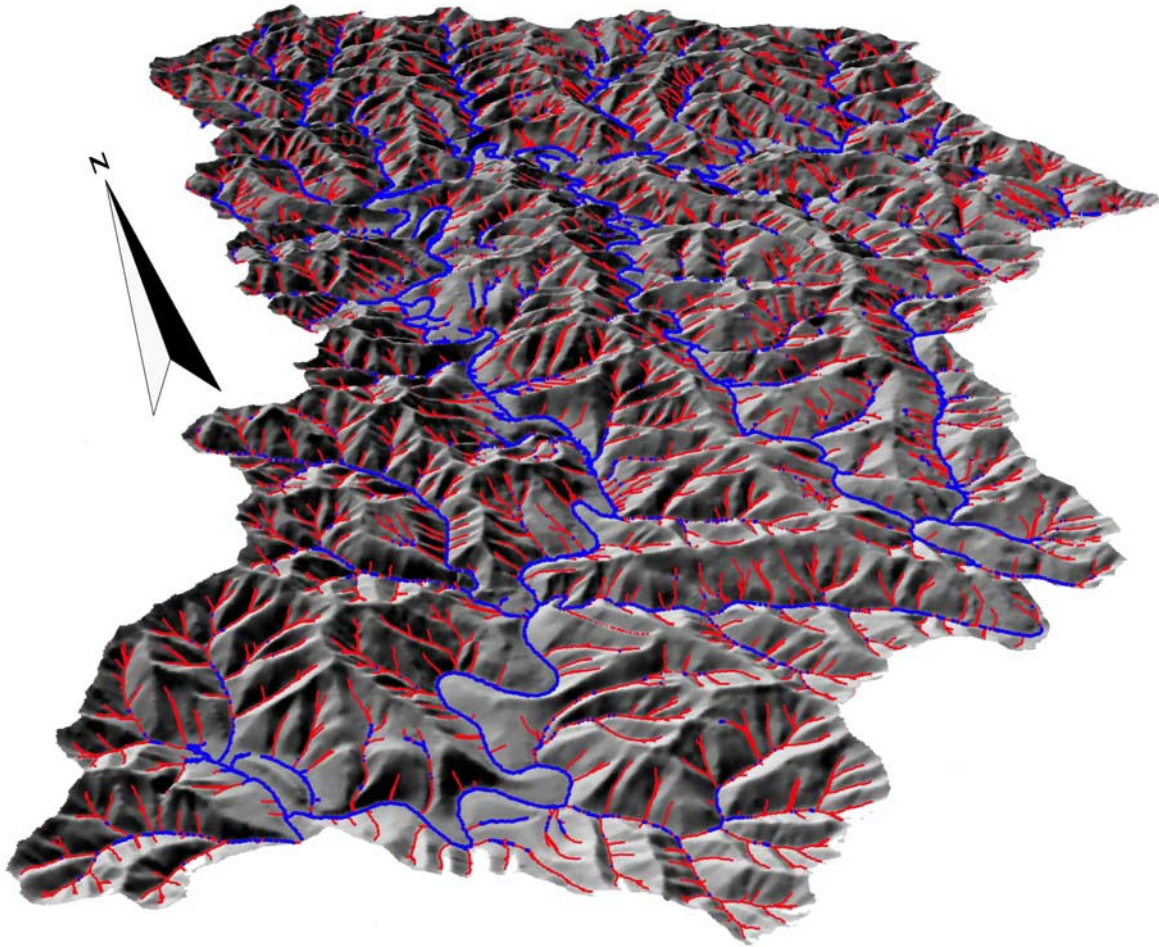
Figure 13. Valley network of the 100-km^2 Millicoma basin, Oregon, extracted from a 10-m DEM. At a drainage area threshold of 1000 m^2, 90% of the valley network length is above 0.10 gradients where debris flows are known to occur.

lished that fluvial processes play no role in steepland valley incision. Rather, we find that the tendency for rapid burial of valley floors after debris flows precludes the widespread occurrence of fluvial incision along debris flow run outs. In field areas where sediment cover is absent and flow occurs, fluvial incision at steep slopes might give rise to a different signature (e.g., Marecchia).

6.1.   Implication of Scaling Transition

[47] Large fractions of valley relief (25–75%) lie above the scaling break at the river valley head for basins that we investigated in Table 3, in reaches steep enough to transport debris flows. Although increasing basin size and distance from base-level (hence average slope) reduce this fraction, it is still substantial even for large basins far away from coasts (e.g., Toplodolska, Vistula, St. Germain). In steep ranges near the coast (e.g., Honeydew, Franklin, Anghou), debris flow valleys are the dominant portions of valley relief (>70%). The location of the transition near the end of debris flow run outs is consistent with a threshold slope beyond which debris flows are not mobile and cannot incise valleys (e.g., Tables 1 and 2). Using 0.10 valley slope as a conservative estimate for this limit, we find that in steep-lands like the Oregon Coast Range, most of the valley network by length, and large fractions of it by relief (Table 3)

are cut by debris flows, not rivers. Figure 13 illustrates this in the 100-km^2 Millicoma basin (from a 10-m DEM kindly provided by Stephen Lancaster, Oregon State University, Corvallis, OR), cut in the Tyee Formation of the Oregon Coast Range. In blue are 10-m valley segments of less than 0.10 slope, a maximum estimate for the extent of fluvial incision. Nonetheless, the red valley network of >0.10 slopes occupies nearly 90% of the channel network length, including much of the local relief. The image indicates that most of the hillslopes in this basin have boundary lowering rates that are set predominately by debris flow incision, not fluvial lowering, and that much of the landscape relief resides in valleys cut by debris flows.

[48] Figure 14 shows profiles for three basins where we have identified process transitions in the field and scaling breaks on area-slope plots. The scaling break in the area-slope plots for each basin occurs at the intersection of the dashed lines with the existing long-profile (solid line). Above the intersection, the valley has a curved area-slope plot that we infer represents debris flows incision. For these basins, debris flow portions of the main stem valley occupy 40–80% of the main stem relief. The dashed lines represent what the profile would look like if the fluvial power law scaling of the lower part of the plots (Figure 10) extended to the valley head defined by contour direction angle. They indicate the role that
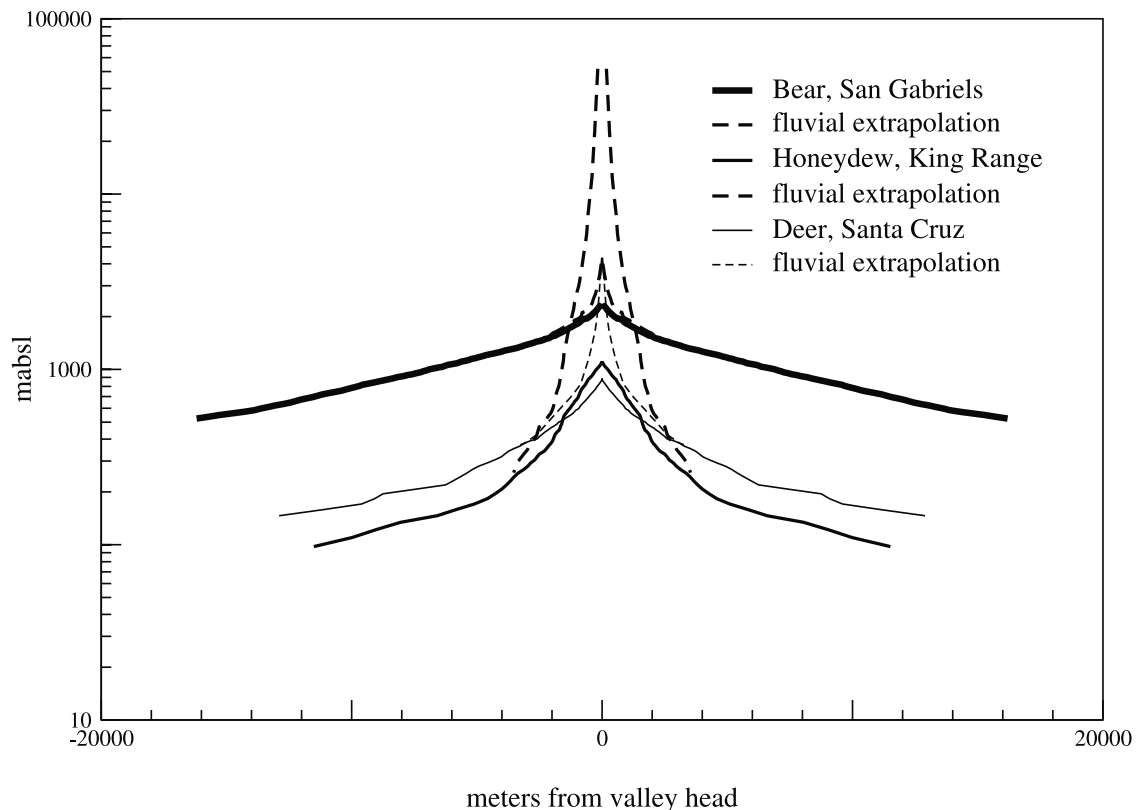
Figure 14. Plot of profiles from Bear, Honeydew, and Deer Creek indicating that much of the valley relief lies in debris flow region. Shown for comparison are profiles predicted by extending slopes predicted by river incision law to valley head (defined by planform curvature from topographic maps).

debris flows have in controlling existing valley relief, although other processes like deep-seated landsliding would probably occur before valleys reached these extreme slopes.

[49] Figure 14 and the fraction of valley relief above river valley heads (Table 3) illustrate that a debris flow incision law, as yet unknown, determines much of the main stem relief and most of the tributary relief for unglaciated steeplands. This means that there is much yet to be learned about the evolution of steep escarpments, river valley walls, and the persistence of topography in orogens, all of which are commonly characterized by valleys with slopes greater than 0.10. Likewise, the influence of climate and erosion rate on relief will require some assessment of the role of debris flows. The transition zone between fluvial and debris flow valley incision, where debris flow material accumulates in the short term, also remains a problematic region about which we know very little.

6.2. Interpretation of Curvature

[50] Fits of equation (5) to U.S. and global debris flow valley profiles have substantial variability, as shown by the range of parameters in Tables 2 and 3. Some of the variation is likely a size effect, with smaller catchments having higher curvature as their longitudinal profiles curve rapidly to join main stems. This size effect in itself indicates that equation (5) does not adequately capture all of the relevant effects controlling curvature.

[51] Other variations in area-slope curvature may reflect response to boundary lowering rates. For instance, catchments on either side of the knickpoint in Sullivan Creek have different curvature (e.g., number 1 versus number 2 in

Table 2) that may reflect a transient response. Steady state responses to rock uplift rates and lithology may also influence curvature.

[52] For instance, Figure 15 summarizes hypotheses about valley response to variations in rock uplift rate and lithology, based on inverse correlation between a_1 and erosion rate that we observe for some basins of similar lithology in Table 3. Valleys cut by debris flows are shown as dashed lines and solid lines show river-cut valleys. While river valleys follow a power law that translates upward with rock uplift rate, debris flow valley slopes in Figure 15a converge to an upper limit within the range of slopes commonly reported for hollows in soil-mantled landscapes. By visual analogy to the string of a bow, Figure 15 shows the debris flow curve pulled upwards and toward greater drainage areas as erosion rates increase, but pinned below slopes at which landslides initiate. This is consistent with the observation that in most of the basins in Figure 12, valley heads reach a limiting slope at vanishingly small drainage areas that is seemingly insensitive to rock uplift rate. This value is near the friction angle for many soils, and is likely set by landslide initiation at hollows, 20–100 m below the ridgeline in our examples. We cannot say whether the upper threshold slope is set by material properties, or the maintenance of slopes above which debris flow incision is extraordinarily rapid. At the other end of the profile, the bowstring is pinned by the lowermost slope values at which debris flows tend to deposit in confined valleys, often slopes of 0.03–0.10. Here there is occasionally an abrupt increase in slope at the upstream end of the linear fluvial trend (see
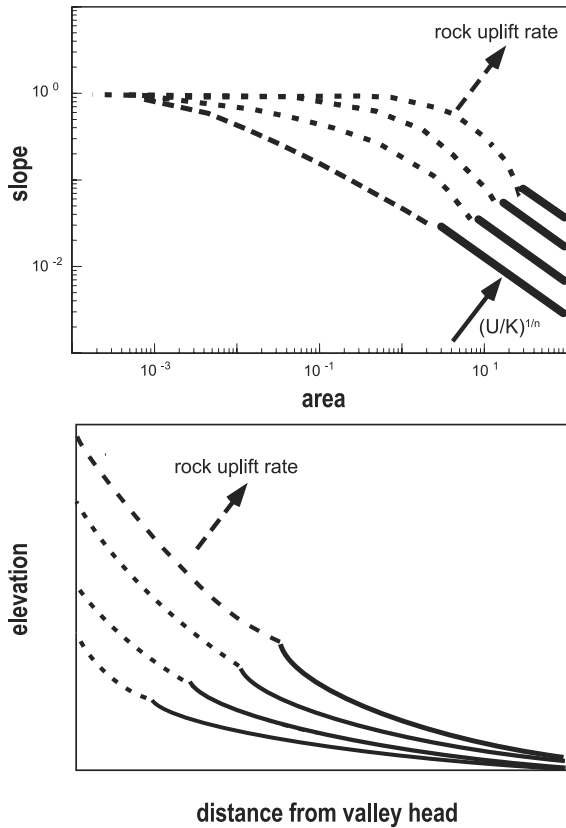
Figure 15. Hypothetical response of valley network to variations in rock uplift rate/rock resistance ratio. As rock uplift rates increase, river valley slopes (solid lines) increase as intercept of the power law translates upward. Debris flow valley slopes (dashed lines) also become steeper resulting in a more linear long profile.

for instance Deer, Cook, Djemaa) leading to a profile steepening at the river valley head.

[53] As rock uplift rates increase, we hypothesize that there is a tendency for lower threshold slopes to migrate to successively larger drainage areas (e.g., Yucaipa, Honeydew). Similar tendencies have been predicted for fluvial systems by the models of *Howard* [1997] and *Tucker and Bras* [1998]. For debris flow cut valleys, this would focus both long-profile and area-slope curvature in the remaining region above the river valley head, resulting in nearly linear upper long-profiles that curve rapidly concave upwards approaching the river valley head. This region of response to rock uplift rates is consistent with the finding by *Merrits and Vincent* [1989] that first order channels respond most sensitively to rock uplift rates, because their blue-line first order channels occur at drainage areas of ~0.1 to 1 km^2, within the highly curved lower section of debris flow area-slope data where small changes in curvature lead to large changes in slope. For the purposes of illustrating this hypothesis, we compare area-slope data from predominately sandstone basins with erosion rates ranging from ~0.01 to 4 mm/yr (Figure 16a). For these basins, area-slope data are more curved at high erosion rates (e.g., Honeydew Creek) compared to low erosion rates (e.g., Knawls Creek, West

Virginia). Hypothetical differences between tectonically active areas and passive ones can also be illustrated by comparing granite basins with little active tectonism (Korea) to those with high erosion rates (San Gabriels) in Figure 16b. Here again there is higher curvature in the debris flow region where erosion rates are higher.

[54] We hypothesize that there is also an influence of lithology on valley profile. Figure 17 illustrates that for roughly equivalent erosion rates, valleys in crystalline rocks like gneisses and granites may be steeper for a given drainage area than those cut in sandstones. Valleys in crystalline rocks or indurated rocks like basalts may also tend to have lower curvatures in the debris flow region (as reflected in larger a_1 values in Table 3) than valleys in sedimentary rocks for similar erosion rates (Figures 17a and 17b).

6.3. Implications for Stream Power Law Exponents

[55] Our comparisons of USGS 30-m data to hand-extracted 1:24,000 data and to laser altimetry indicate that scatter in the 30-m data obscure scaling transitions and do not exactly reproduce source data parameters (e.g., m/n
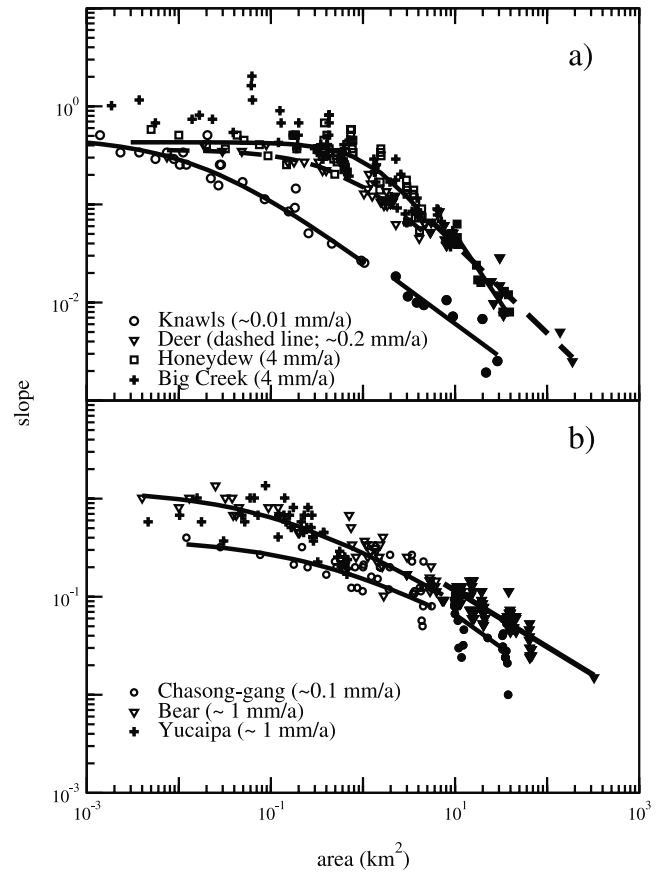
Figure 16. Apparent effect of rock uplift rates on valley slope in (a) sandstone basins, Knawls Creek, (West Virginia) and Deer Creek, Santa Cruz Mountains, and Honeydew (California), and (b) granitic basins, Chasong-gang, North Korea, and Bear Creek, San Gabriels, California. Solid symbols are data that follow a fluvial, linear power law (see text for details). Open symbols are curved, reflecting debris flow valley incision. See Table 3 for fit parameters.
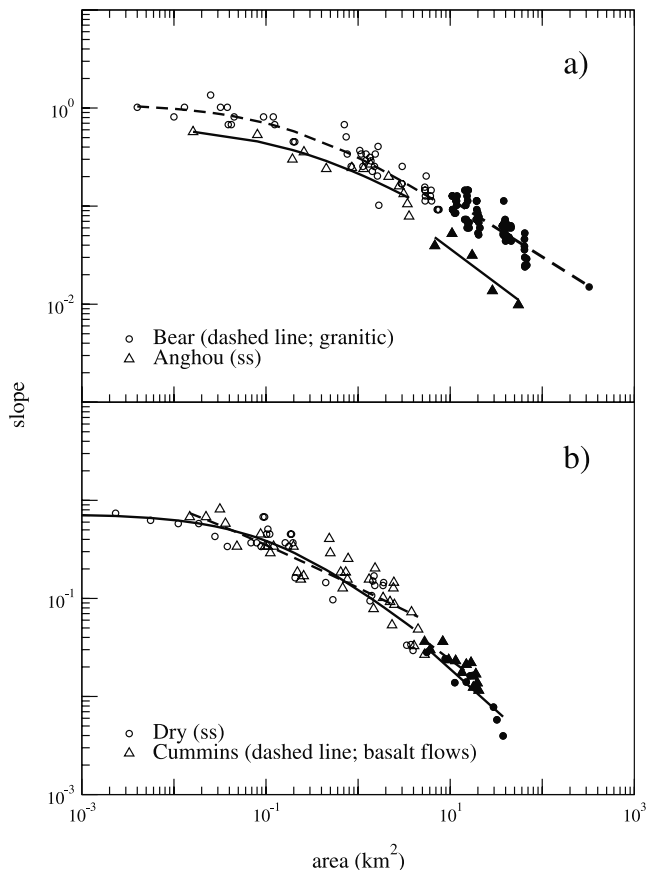
Figure 17. Apparent effect of lithology on valley form. Solid symbols are data that follow a fluvial, linear power law (see text for details). Open symbols are curved, reflecting debris flow valley incision. See Table 3 for parameters of both fits. Valleys in crystalline or indurated rocks (e.g., some basalts) tend to have lower long-profile curvature in both fluvial and debris flow regions. This is reflected in lower m/n values for granites and basalts versus sandstones at similar rock uplift rates, and higher values of a_1 in the debris flow region (indicating lower curvature) for crystalline rocks and basalts versus sandstones.

values). At low drainage areas (e.g., $<10^{-4}$ km^2) much of the network may be artifactual, while at larger areas slope scatter is substantial. Therefore 30-m DEMs used for area-slope analysis need to be validated by comparing them to the 1:24,000 quadrangle source before they can be used to infer scaling laws. Great care should be taken to ensure that the data being fit with power laws are indeed linear in log-log space. For instance, inclusion of data that curve at low drainage areas in power law regressions decreases m/n values and increases intercept $[(-\partial z/\partial t)/K]^{1/n}$ values (e.g., Figure 7). This could lead to spurious correlations between rock uplift rate and power law slope and intercept. To avoid this problem, headwater reaches above 0.03 slope should be excluded from stream power law analysis unless they are demonstrably influenced by fluvial incision (e.g., presence of strath terraces or extension of well-defined single power law).

[56] Even m/n values extracted only from fluvial regions vary substantially in Table 3. For instance, basins that follow a single power law exceedingly well (R^2 values > 0.9) have m/n values that vary from 0.7–1.0 for sedimen-

tary and metamorphic lithologies. Valleys in hard, crystalline rocks like granites tend to have m/n values (0.4–0.6) lower than those of valleys in sedimentary rocks, but this might also be an artifact of the small number of valleys we measured in granitic rocks. The range of m/n values in Table 3 spans those reported in the literature, from high values like 1.0 [*Seidl and Dietrich*, 1992; *Seidl et al.*, 1994], to lower values like 0.1– 0.5 [*Stock and Montgomery*, 1999; *Snyder et al.*, 2000]. We have not established that each basin has uniform lithology or is at steady state, but this variation in m/n indicates that there is no single m/n value that can be extracted from topographic data for a general stream power law.

7. Conclusions

[57] Field observations and map analysis demonstrate that debris flows that occur in landscapes steep enough to produce mass failures both erode bedrock and have a topographic signature in the form of curvature in area-slope space above 0.03–0.10 slope. Power law plots of slope versus area, widely used to examine bedrock river incision laws, begin to over-predict valley slopes just upstream of the last strath terrace. Above this region, the influence of debris flows increases rapidly, and is reflected in a curved relation between slope and area on log-log plots that corresponds to mapped debris flow run outs. This topographic signature is consistent with a fundamentally different valley incision law by debris flows, whose form we further explore in a forthcoming paper. Much of the world's steepland valleys, similar in planform appearance to fluvial networks, may be cut by debris flows. Debris flow networks are relevant to landscape evolution because they are both extensive by length (>80% of large steepland basins) and comprise large fractions of main stem valley relief (25– 100%). As a consequence, valleys that are predominately carved by debris flows, not rivers, bound most hillslopes in unglaciated steeplands. Debris flows limit the relief of unglaciated mountain ranges to substantially lower elevations than river incision laws would predict. Together these observations demonstrate that a debris flow incision law is needed to explore mechanistic linkages between tectonics, climate, and topography in unglaciated steeplands.

References

Alford, D., Streamflow and sediment transport from mountain watersheds of the Chao Phraya basin, northern Thailand: A reconnaissance study, *Mountain Res. Dev.*, *12*, 257–268, 1992.

Anderson, R. S., Evolution of the Santa Cruz Mountains, California, through tectonic growth and geomorphic decay, *J. Geophys. Res.*, *99*, 20,161–20,179, 1994.

Ando, N., K. Terazono, and R. Kitazume, Sediment removal project at Miwa dam, paper presented at Dix-huitieme Congres des Grandes Barrages, Comm. Int. des Grands Barrages, Durban, South Africa, 1994.

Armstrong, P. A., T. A. Ehlers, D. S. Chapman, K. A. Farley, and P. J. J. Kamp, Exhumation of the central Wasatch Mountains: Constraints from

low-temperature thermochronometry, *Eos Trans. AGU*, *80* Fall Meet. Suppl, F1034 1999.

Bagnold, R. A., An approach to the sediment transport problem from general physics, *U.S. Geol. Surv. Prof. Pap.*, *422-I*, 1966.

Benda, L. E., The influence of debris flows on channels and valley floors in the Oregon Coast Range, U.S.A., *Earth Surf. Processes*, *15*, 457–466, 1990.

Benda, L., and T. W. Cundy, Predicting deposition of debris flows in mountain channels, *Can. Geotech. J.*, *27*, 409–417, 1990.

Benda, L., and T. Dunne, Stochastic forcing of sediment supply to channel networks from landsliding and debris flows, *Water Resour. Res.*, *33*, 2849–2863, 1997.

Berti, M., R. Genevois, A. Simoni, and P. R. Tecca, Field observations of a debris flow event in the Dolomites, *Geomorphology*, *29*, 265–274, 1999.

Blythe, A. E., D. W. Burbank, K. A. Farley, and E. J. Fielding, Structural and topographic evolution of the central Transverse Ranges, California, from apatite fission-track, (U-Th)/He and digital elevation model analyses, *Basin Res.*, *12*, 97–114, 2000.

Brown III, W. M., Erosion processes, fluvial sediment transport, and reservoir sedimentation in a part of the Newell and Zayante Creek basins, Santa Cruz County, California, *U.S. Geol. Surv. Open File Rep.*, *73-35*, 1973.

Campbell, R. H., Soil slips, debris flows, and rainstorms in the Santa Monica Mountains and vicinity, southern California, *U.S. Geol. Surv. Prof.*, *851*, 1975.

Carter, A., D. Roques, and C. S. Bristow, Denudation history of onshore central Vietnam: Constraints on the Cenozoic evolution of the western margin of the South China Sea, *Tectonophysics*, *322*, 265–277, 2000.

Cenderelli, D. A., and J. S. Kite, Geomorphic effects of large debris flows on channel morphology at North Fork Mountain, eastern West Virginia, USA, *Earth Surf. Processes Landforms*, *23*, 1–19, 1998.

Coats, R., L. Collins, J. Florsheim, and D. Kaufman, Landsliding, channel change, and sediment transport in Zayante Creek and the lower San Lorenzo River, 1982 water year, and implications for management of the stream resource, report, State Water Resources Control Board, Water Resour. Cent. Archive, U. C. Berkeley, 1982.

Coltorti, M., and C. D. Ollier, Geomorphic and tectonic evolution of the Ecuadorian Andes, *Geomorphology*, *32*, 1–19, 2000.

Coltorti, M., and P. Pieruccini, A late Lower Miocene planation surface across the Italian Peninsula: A key tool in neotectonic studies, *J. Geodyn.*, *29*, 323–328, 2000.

Costa, J. E., Physical geomorphology of debris flows, in *Developments and Applications of Geomorphology*, edited by J. E. Costa and P. J. Fleisher, Springer-Verlag, New York, 1984.

Curry, R. R., Observation of alpine mudflows in the Tenmile Range, central Colorado, *Geol. Soc. Am. Bull.*, *77*, 771–776, 1966.

Davis, W. M., River terraces in New England, *Bull. Mus. Comp. Zool.*, *38*, 281–346, 1902.

Davy, P., and A. Crave, Upscaling local-scale transport processes in large-scale relief dynamics, *Phys. Chem. Earth A*, *25*, 533–541, 2000.

Dendy, F. E., and W. A. Champion, Sediment deposition in U. S. reservoirs, Summary of data reported through 1975, *U.S. Dep. Agric. Misc. Publ.*, *1362*, 1978.

Dietrich, W. E., and T. Dunne, Sediment budget for a small catchment in mountainous terrain, *Z. Geomorphol. Suppl.*, *29*, 191–206, 1978.

Errih, M., and H. Bendahou, Desilting of water reservoirs in Algeria by dredging, study case: The Fergug reservoir, in *Energy and Water: Sustainable Development, Proceedings of Theme D, 27th Congress of the IAHR*, pp. 132–137, Am. Soc. of Civ. Eng., New York, 1997.

Fannin, R. J., and T. P. Rollerson, Debris flows: Some physical characteristics and behaviour, *Can. Geotech. J.*, *30*, 71–81, 1993.

Flint, J. J., Stream gradient as a function of order, magnitude, and discharge, *Water Resour. Res.*, *10*, 969–973, 1974.

Gay, I., and J.-J. Macaire, Estimation of late glacial and Holocene chemical erosion rates, Lake Chambon watershed, Massif Central, France, *Surf. Geosci.*, *328*, 387–392, 1999.

Gilbert, G. K., *Report on the Geology of the Henry Mountains*, U.S. Gov. Print. Off., Washington, D. C., 1877.

Heimsath, A. M., W. E. Dietrich, K. Nishiizumi, and R. C. Finkel, Stochastic processes of soil production and transport: Erosion rates, topographic variation, and cosmogenic nuclides in the Oregon Coast Range, *Earth Surf. Processes Landforms*, *26*, 531–552, 2001.

Horton, R. E., Erosional development of streams and their drainage basins; hydrophysical approach to quantitative morphology, *Geol. Soc. Am. Bull.*, *56*, 275–370, 1945.

Howard, A. D., A detachment-limited model of drainage basin evolution, *Water Resour. Res.*, *30*, 2261–2285, 1994.

Howard, A. D., Badland morphology and evolution: Interpretation using a simulation model, *Earth Surf. Processes Landforms*, *22*, 211–227, 1997.

Howard, A. D., Long profile development of bedrock channels: Interaction of weathering, mass wasting, bed erosion, and sediment transport, in *Rivers Over Rock: Fluvial Processes in Bedrock Channels*, *Geophys. Monogr. Ser.*, vol. 107, edited by K. J. Tinkler and E. E. Wohl, pp. 297–319, AGU, Washington, D. C., 1998.

Howard, A., and G. Kerby, Channel changes in badlands, *Geol. Soc. Am. Bull.*, *94*, 739–752, 1983.

Hungr, O., G. C. Morgan, and R. Kellerhals, Quantitative analysis of debris torrent hazards for design of remedial measures, *Can. Geotech. J.*, *21*, 663–677, 1984.

Ijjasz-Vasquez, E. J., and R. L. Bras, Scaling regimes of local slope versus contributing area in digital elevation models, *Geomorphology*, *12*, 299–311, 1995.

Ikeya, H., Debris flow and its countermeasures in Japan, *Bull. Int. Assoc. Eng. Geol.*, *40*, 5–33, 1989.

Iverson, R. M., The physics of debris flows, *Rev. Geophys.*, *35*, 245–296, 1997.

Jantawat, S., An overview of soil erosion and sedimentation in Thailand, in *Soil Erosion and Conservation*, edited by S. A. El-Swaify, W. C. Moldenhauer, and A. Lo, pp. 10–14, Soil Conserv. Soc. of Am., Ankeny, Iowa, 1985.

Kirby, E., and K. X. Whipple, Quantifying differential rock-uplift rates via stream profile analysis, *Geology*, *29*, 415–418, 2001.

Kooi, H., and C. Beaumont, Large-scale geomorphology: classical concepts reconciled and integrated with contemporary ideas via a surface processes model, *J. Geophys. Res.*, *101*, 3361–3386, 1996.

Kostadinov, S., and S. Markovic, Soil erosion and effects of erosion control works in the torrential drainage basins of southeast Serbia, in *Erosion and Sediment Yield: Global and Regional Perspectives*, edited by D. E. Walling and B. W. Webb, *IAHS Publ.*, *236*, 321–332, 1996.

Lague, D., P. Davy, and A. Crave, Estimating uplift rate and erodibility from the area-slope relationship: Examples from Brittany (France) and numerical modelling, *Phys. Chem. Earth A*, *25*, 543–548, 2000.

Lajczak, A., Sediment yield within the upper Vistula catchment, in *Evolution of the Vistula River Valley During the Last 15,000 Years*, part III, *Geogr. Stud. Spec. Issue*, vol. 5, edited by L. Starkel, pp. 90–95, Polish Acad. of Sci., Wroclaw, 1990.

Larsson, S., Geomorphological effects on the slopes of Longyear valley, Spitsbergen, after a heavy rainstorm in July 1972, *Geogr. Ann.*, *64A*, 105–125, 1982.

Laubacher, G., and C. W. Naeser, Fission-track dating of granitic rocks from the Eastern Cordillera of Peru: Evidence for Late Jurassic and Cenozoic cooling, *J. Geol. Soc.*, *151*, 473–483, 1994.

Lewin, J., and J. Warburton, Debris flow in an alpine environment, *Geogr. J. Geogr. Assoc.*, *343*, 98–107, 1994.

Li, Y.-H., Denudation of Taiwan Island since the Pliocene epoch, *Geology*, *4*, 105–107, 1976.

Lim, H. S., and Y. I. Lee, Thermal history of the Cretaceous Sindong Group, Korea from fission-track analysis, *Geosci. J.*, *4*, 52–56, 2000.

Liu, T.-K., S. Hsieh, Y.-G. Chen, and W.-S. Chen, Thermo-kinematic evolution of the Taiwan oblique-collision mountain belt as revealed by zircon fission track dating, *Earth Planet. Sci. Lett.*, *186*, 45–56, 2001.

Maluski, H., C. Lepvrier, L. Jolivet, A. Carter, D. Roques, O. Beyssac, T. T. Tang, N. D. Thang, and D. Avigad, Ar-Ar and fission-track ages in the Song Chay Massif: Early Triassic and Cenozoic tectonics in northern Vietnam, *J. Asian Earth Sci.*, *19*, 233–248, 2001.

Maneux, E., J. L. Probst, E. Veyssy, and H. Etcheber, Assessment of dam trapping efficiency from water residence time: Application to fluvial sediment transport in the Adour, Dordogne, and Garonne River basins (France), *Water Resour. Res.*, *37*, 801–811, 2001.

Merritts, D., and K. R. Vincent, Geomorphic response of coastal streams to low, intermediate, and high rates of uplift, Mendocino triple junction region, northern California, *Geol. Soc. Am. Bull.*, *101*, 1373–1388, 1989.

Moglen, G. E., and R. L. Bras, The importance of spatially heterogenous erosivity and the cumulative area distribution within a basin evolution model, *Geomorphology*, *12*, 173–185, 1995.

Montgomery, D. R., and J. M. Buffington, Channel-reach morphology in mountain drainage basins, *Geol. Soc. Am. Bull.*, *109*, 596–611, 1997.

Montgomery, D. R., and E. Foufoula-Georgiou, Channel network source representation using digital elevation models, *Water Res. Res.*, *29*, 3925–3934, 1993.

Morel, J. L., and M. Meghraoui, Goringe-Alboran-Tell tectonic zone: A transpression system along the Africa-Eurasia plate boundary, *Geology*, *24*, 755–758, 1996.

Morgan, B. A., G. F. Wieczorek, and R. H. Campbell, Map of rainfall, debris flows, and flood effects of the June 27, 1995, storm in Madison County, Virginia, *U.S. Geol. Surv. Map, I-2623-A*, 1999.

Morton, D. H., and R. Campbell, Spring mudflows at Wrightwood, southern California, *Q. J. Eng. Geol.*, 7, 377–384, 1974.

Munoz, N., and R. Charrier, Uplift of the western border of the Altiplano on a west-vergent thrust system, northern Chile, *J. S. Am. Earth Sci.*, 9, 171–181, 1996.

Perg, L., R. S. Anderson, and R. Finkel, Cosmogenic radionuclide constraints on the long-term sediment budget of the Santa Cruz littoral cell, California, USA, *Eos Trans. AGU*, 81(48), Fall Meet. Suppl., abstract U21A-24 2000.

Personious, S. F., Late Quaternary stream incision and uplift in the forearc of the Cascadia subduction zone, western Oregon, *J. Geophys. Res.*, 100, 20,193–20,210, 1995.

Petkovic, S., N. Dragovic, and S. Markovic, Erosion and sedimentation problems in Serbia, *Hydrol. Sci. J.*, 44, 63–77, 1999.

Pierson, T. C., Erosion and deposition by debris flows at Mt. Thomas, North Canterbury, New Zealand, *Earth Surf. Proc.*, 5, 227–247, 1980.

Playfair, J., *Illustrations of the Huttonian Theory of the Earth*, Dover, Mineola, N. Y., 1802.

Poulos, S. E., M. Collins, and G. Evans, Water-sediment fluxes of Greek rivers, southeastern Alpine Europe: Annual yields, seasonal variability, delta formation and human impact, *Z. Geomorphol.*, 40, 243–261, 1996.

Rapp, A., and R. Nyberg, Alpine debris flows in northern Scandinavia, *Geogr. Ann.*, 63A, 183–196, 1981.

Reneau, S. L., and W. E. Dietrich, Erosion rates in the southern Oregon Coast Range: Evidence for equilibrium between hillslope erosion and sediment yield, *Earth Surf. Processes Landforms*, 16, 307–322, 1991.

Rickenmann, D., and M. Zimmermann, The 1987 debris flows in Switzerland: Documentation and analysis, *Geomorphology*, 8, 175–189, 1993.

Roe, G. H., D. R. Montgomery, and B. Hallet, Effects of orographic precipitation on the concavity of steady-state river profiles, *Geology*, 30, 143–146, 2002.

Roering, J. J., J. W. Kirchner, and W. E. Dietrich, Identification and characterization of deep-seated landslides in the Oregon Coast Range using digital terrain data, *Eos Trans. AGU*, 77, 246, 1996.

Roessner, S., and M. R. Strecker, Late Cenozoic tectonics and denudation in the Central Kenya Rift: Quantification of long-term denudation rates, *Tectonophysics*, 278, 83–94, 1997.

Rosenbloom, N. A., and R. S. Anderson, Hillslope and channel evolution in a marine terraced landscape, Santa Cruz, California, *J. Geophys. Res.*, 99, 14,013–14,029, 1994.

Salas, C. A., R. C. Rayan, E. S. Montero, and J. L. G. Montana, Sediment yield at Spanish reservoirs and its relationship with the drainage basin area, paper presented at Dix-neuvieme Congres des Grandes Barrages, Comm. Int. des Grands Barrages, Florence, Italy, 1997.

Scott, K. M., Origin and sedimentology of 1969 debris flows near Glendosa, California, *U.S. Geol. Surv. Prof. Pap.*, 750-C, 242–247, 1971.

Seidl, M. A., and W. E. Dietrich, The problem of channel erosion into bedrock, in *Functional Geomorphology*, edited by K.-H. Schmidt and J. DePloey, *Catena Suppl.*, 23, 101–124, 1992.

Seidl, M. A., W. E. Dietrich, and J. W. Kirchner, Longitudinal profile development into bedrock: An analysis of Hawaiian channels, *J. Geol.*, 102, 457–474, 1994.

Serrat, P., Present sediment yield from a Mediterranean fluvial system: The Agly river (France), *Surface Geosci.*, 329, 189–196, 1999.

Sharpe, R. P., and L. H. Nobles, Mudflow of 1941 at Wrightwood, southern California, *Geol. Soc. Am. Bull.*, 64, 547–560, 1953.

Sklar, L., and W. E. Dietrich, River longitudinal profiles and bedrock incision models: Stream power and the influence of sediment supply, in *Rivers Over Rock: Fluvial Processes in Bedrock Channels*, Geophys. Monogr. Ser., vol. 107, edited by K. J. Tinkler and E. E. Wohl, pp. 237–260, AGU, Washington, D. C., 1998.

Sklar, L. S., and W. E. Dietrich, Sediment and rock strength controls on river incision into bedrock, *Geology*, 29, 1087–1090, 2001.

Snyder, N. P., K. X Whipple, G. E. Tucker, and D. J. Merritts, Landscape response to tectonic forcing: Digital elevation model analysis of stream profiles in the Mendocino triple junction region, northern California, *Geol. Soc. Am. Bull.*, 112, 1250–1263, 2000.

Sorriso-Valvo, M., L. Antronico, and E. Le Pera, Controls on fan morphology in Calabria, southern Italy, *Geomorphology*, 24, 169–187, 1998.

Spotila, J. A., K. A. Farley, J. D. Yule, and P. W. Reiners, Rapid, long-lived exhumation along the transpressive San Andreas Fault Zone in southern California, based on U-Th/He dating, *Eos Trans. AGU*, 80 Fall Meet. Suppl., F1170, 1999.

Steinmann, M., D. Hungerbuhler, D. Seward, and W. Winkler, Neogene tectonic evolution and exhumation of the southern Ecuadorian Andes: A combined stratigraphy and fission-track approach, *Tectonophysics*, 307, 255–276, 1999.

Stock, J. D., and D. R. Montgomery, Geologic constraints on bedrock river incision using the stream power law, *J. Geophys. Res.*, 104, 4983–4993, 1999.

Suwa, H., and S. Okuda, Deposition of debris flows on a fan surface Mt. Yakedake, Japan, *Z. Geomorphol. Suppl.*, 46, 79–101, 1983.

Swanson, F. J., and G. W. Lienkaemper, Physical consequences of large organic debris in Pacific Northwest streams, *U.S. For. Serv. Gen. Tech. Rep.*, PNW-69, 1978.

Takemura, K., O. Arai, N. Fujita, and M. Sakaue, Prevention of reservoir sedimentation in Japan, paper presented at Dix-nuvieme Congres des Grandes Barrages, Comm. Int. des Grands Barrages, Florence, Italy, 1997.

Tucker, G. E., and R. L. Bras, Hillslope processes, drainage density, and landscape morphology, *Water Resour. Res.*, 34, 2751–2764, 1998.

Tucker, G. E., and R. L. Slingerland, Erosional dynamics, flexural isostasy, and long-lived escarpments: A numerical modeling study, *J. Geophys. Res.*, 99, 12,229–12,243, 1994.

Tucker, G. E., and R. L. Slingerland, Drainage basin response to climate change, *Water. Resour. Res.*, 33, 2031–2047, 1997.

van der Beek, P., and J. Braun, Controls on post mid-Cretaceous landscape evolution in the southeastern highlands of Australia: Insights from numerical suface process models, *J. Geophys. Res.*, 104, 4945–4996, 1999.

van der Meulen, M. J., T. J. Kouwenhove, G. J. van der Zwaan, J. E. Meulenkamp, and M. J. R. Wortel, Late Miocene uplift of the Romagnan Apennines and the detachment of subducted lithosphere, *Tectonophysics*, 315, 319–335, 1999.

VanDine, D. F., Debris flows and debris torrents in the southern Canadian Cordillera, *Can. Geotech. J.*, 22, 44–68, 1985.

Van Steijn, H., J. de Ruig, and F. Hoozemans, Morphological and mechanical aspects of debris flows in parts of the French Alps, *Z. Geomorphol.*, 32, 143–161, 1988.

Verges, J., H. Millan, E. Roca, J. A. Munoz, M. Marzo, J. Cires, T. Den Bezemer, R. Zoetemeijer, and S. Cloetingh, Eastern Pyrenees and related foreland basins: pre-, syn-, and post-collisional crustal-scale cross-sections, *Mar. Petrol. Geol.*, 12, 893–915, 1995.

Walling, D. E., and B. W. Webb, Erosion and sediment yield: A global overview, in *Erosion and Sediment Yield: Global and Regional Perspectives*, edited by D. E. Walling and B. W. Webb, *IAHS Publ.*, 236, 3–19, 1996.

Whipple, K. X, and G. E. Tucker, Dynamics of the stream-power river incision model: Implications for height limits of mountain ranges, landscape response timescales, and research needs, *J. Geophys. Res.*, 104, 17,661–17,674, 1999.

Whipple, K. X, E. Kirby, and S. H. Brocklehurst, Geomorphic limits to climate-induced increases in topographic relief, *Nature*, 401, 39–43, 1999.

Whipple, K. X, N. P. Snyder, and K. Dollenmayer, Rates and processes of bedrock incision by the Upper Ukak River since the 1912 Novarupta ash flow in the Valley of Ten Thousand Smokes, Alaska, *Geology*, 28, 835–838, 2000.

White, S., Sediment yield and availability for two reservoir drainage basins in central Luzon, Philippines, in *Sediment Budgets*, *IAHS Publ.*, 174, 575–581, 1988.

Willett, S. D., R. Slingerland, and N. Hovius, Uplift, shortening, and steady state topography in active mountain belts, *Am. J. Sci.*, 301, 455–485, 2001.

Willgoose, G., R. L. Bras, and I. Rodriguez-Iturbe, Results from a new model of basin evolution, *Earth Surf. Processes Landforms*, 16, 237–254, 1991.

Williams, S. R., and M. Lowe, Process-based debris-flow prediction method, in *Hydraulics/Hydrology of Arid Lands (H2AL)*, edited by R. H. French, pp. 66–71, Am. Soc. of Civ. Eng., New York, 1990.

Wohl, E., and P. P. Pearthree, Debris flows as geomorphic agents in the Huachuca Mountains of southwestern Arizona, *Geomorphology*, 4, 273–292, 1991.

Wooley, R. R., Cloudburst floods in Utah, 1850–1938, *U.S. Geol. Surv. Water Supply Pap.*, 994, 1946.

Yatsu, E., On the profile of the graded river, *Eos Tran. AGU*, 36, 211–219, 1955.

Yoon, B., and H. Woo, Sediment problems in Korea, *J. Hydraul. Eng.*, 126, 486–491, 2000.

W. E. Dietrich and J. Stock, Department of Earth and Planetary Sciences, University of California, 307 McCone, Berkeley, CA 94720, USA. (jdstock@geomorph.berkeley.edu)